2009

Exploring Factors Controlling the Thermal Behavior of Ammonium Perchlorate and Ammonium Nitrate Energetic Systems

Anthony Justin Lang
University of Alabama at Birmingham

EXPLORING FACTORS CONTROLLING THE THERMAL BEHAVIOR OF AMMONIUM PERCHLORATE AND AMMONIUM NITRATE ENERGETIC SYSTEMS

by

ANTHONY J. LANG

SERGEY VYAZOVKIN, CHAIR
DERRICK R. DEAN
TRACY P. HAMILTON
ANDREI STANISHEVSKY
CHARLES L. WATKINS

A DISSERTATION

Submitted to the graduate faculty of The University of Alabama at Birmingham,
in partial fulfillment of the requirements for the degree of
Doctor of Philosophy

BIRMINGHAM, ALABAMA
2009

EXPLORING FACTORS CONTROLLING THE THERMAL BEHAVIOR OF AMMONIUM PERCHLORATE AND AMMONIUM NITRATE ENERGETIC SYSTEMS

ANTHONY J. LANG

CHEMISTRY

ABSTRACT

This research project characterizes ammonium nitrate (AN) and ammonium perchlorate (AP) to assist in the parameter optimization of ammonium-salt propellants. Throughout these studies, the effective activation energies for thermal events are identified through the application of the Advanced Isoconversional Method. Differential Scanning Calorimetry (DSC), Thermogravimetric Analysis (TGA), High Pressure DSC (HP-DSC), Fourier Transform Infrared Spectroscopy (FTIR), TGA-FTIR evolved gas analysis, density functional calculations, and microscopy techniques were employed to evaluate the systems.

The first article studies the thermal decomposition properties of ammonium perchlorate as a function of sample condition. It was discovered that sublimation and decomposition are dependent on particle size, the density resulting from compression, and the pressured exerted by the sheath gas. The onset of AP's thermal decomposition appears to be similar for all samples, however, the later stages exhibit a significant change in the effective activation energy depending on the sample preparation.

The second and third articles are primarily focused on a novel approach to influence the thermal behavior of AN through the use of polar polymer matrices. Polyvinylpyrrolidone (PVP) and polyacrylamide (PAM) were utilized as hosts for AN. It was discovered that both PAM and PVP forms an amorphous glass with AN when the

respective anion and cation are spatially separated from each other. This separation is achieved though an ion-dipole interaction with the amide located in the functional group of the host polymers. Glass formation was confirmed by the absence of AN's solid-solid phase transitions in the DSC, polarized optical microscopy, and quantum mechanical calculations. It was discovered that PVP and PAM are able to effectively separate the respective ions until the glass transition temperature (Tg) of PVP and the early stages of polymer degradation for PAM at which point a highly exothermic reaction takes place.

Keywords: Ammonium Nitrate, Ammonium perchlorate, Advanced Isoconversional Method, Polyvinylpyrrolidone, Polyacrylamide, DSC

DEDICATION

For Sarah, Mom and Dad

ACKNOWLEDGMENTS

I would like to extend my sincere gratitude to the following individuals: Dr. Sergey Vyazovkin, my mentor and teacher, for all of his leadership and guidance throughout my studies. My graduate committee for keeping me on task and providing direction. Dr. David Graves for his support. UAB Graduate School for allowing me to pursue this work. Dr. Tracy Hamilton for all of his help with my modeling project. Dr. Kai Chen for his assistance with TGA-FTIR and friendship. Dr. Ion Dranca, Tammie Ridley, Laura Knighten, Jackie Nikles , and Cindy Willingham for their friendship and support.

TABLE OF CONTENTS

Page

LIST OF TABLES

Tables *Page*

THE EFFECT OF PRESSURE AND SAMPLE TYPE ON THE DECOMPOSITION OF AMMONIUM PERCHLORATE

AMMONIUM NITRATE-POLYMER GLASSES: A NEW CONCEPT FOR PHASE AND THERMAL STABILIZATION OF AMMONIUM NITRATE

LIST OF FIGURES

Figure *Page*

INTRODUCTION

THE EFFECT OF PRESSURE AND SAMPLE TYPE ON THE DECOMPOSITION OF AMMONIUM PERCHLORATE

PHASE AND THERMAL STABILIZATION OF AMMONIUM NITRATE IN THE FORM OF PVP-AN GLASS

AMMONIUM NITRATE-POLYMER GLASSES: A NEW CONCEPT FOR PHASE AND THERMAL STABILIZATION OF AMMONIUM NITRATE

LIST OF ABBREVIATIONS

α	percent conversion
ADN	Ammonium dinitramide
AN	ammonium nitrate
AP	ammonium perchlorate
AP1900	ammonium perchlorate (particle size)
AP265	ammonium perchlorate (particle size)
AP3	ammonium perchlorate (particle size)
AP4T	ammonium perchlorate pellet (pressure applied)
AP7T	ammonium perchlorate pellet (pressure applied)
DSC	differential scanning calorimetry
e	thermal event
Eα	activation energy
FTIR	Fourier Transform Infrared Spectroscopy
HP-DSC	high pressure differential scanning calorimetry
i	initial time

m	number of intervals chosen for analysis
me	mass loss of an event
M	molecular weight
n	experiment #
PAM	polyacrylamide
PEO	Polyethylene oxide
PVP	polyvinylpyrrolidone
PSAN	phase stabilized ammonium nitrate
PQS	Parallel Quantum Solutions
q	integrated area of DSC peak
Q	heat of reaction
t	time
Ti (t)	temperature program
Tg	glass transition temperature
TGA	thermogravimetric analysis

INTRODUCTION

Background. Ammonium (NH_4^+) based oxidizers are quite popular in the propellant industry. The most widely used being ammonium perchlorate (AP), and to a lesser extent ammonium nitrate (AN). The decomposition of AP as well as other ammonium salts such as AN and ammonium dinitramide (ADN) begin with dissociative sublimation to ammonia and its respective acid[1].

$$NH_4^+A^-_{(s)} \Leftrightarrow NH_{3(g)} + HA_{(g)} \qquad \text{Eq. 1}$$

Once in the gas phase $NH_{3(g)}$ is oxidized by the acid giving rise to various decomposition products that depend on the temperature. Boldyrev[2] recently published an excellent review on the decomposition properties of AP, which identifies the effect of mechanical stresses, temperature, and additives. As seen in equations 2 and 3 based on the temperature, the products of decomposition change.

Decomposition products below 300ºC (Orthorhombic phase):

$$4NH_4ClO_4 \rightarrow 2Cl_{2(g)} + 2N_2O_{(g)} + 3O_{2(g)} + 8H_2O_{(g)} \qquad \text{Eq. 2}$$

(HCl, ClO_2 and N_2 are also formed as a result of secondary reactions)

Decomposition products above 300 ºC (Cubic phase):

$$2NH_4ClO_4 \rightarrow Cl_{2(g)} + 2NO_{(g)} + O_{2(g)} + 4H_2O_{(g)} \qquad \text{Eq. 3}$$

(HCl, NOCl, and NO_2 are also formed as a result of secondary reactions)

Ammonium salts first undergo sublimation (endothermic process), followed by the energetic oxidation of ammonia by the acid (exothermic process). The stability of the oxidizer is controlled by the anion. If the anion is thermally unstable it may decompose before the salt undergoes any appreciable sublimation. This is the case of ADN, whose

decomposition is highly exothermic when decomposed in an open system and under a nitrogen stream[3]. Conversely, the heating of AN under similar conditions results exclusively in endothermic sublimation[4].

AP is most often used because it is stable, both in terms of reactivity and shelf life under ambient conditions. In an inert atmosphere at ambient pressure, it undergoes one solid-solid (orthorhombic/cubic) phase transition at 240 ºC, followed by decomposition, which achieves its maximum rate before 350 ºC [2]. AP doesn't significantly absorb atmospheric water and is easy to blend with burn rate modifiers and fuels such as hydroxy-terminating polybutadiene (HTPB.) Despite the vast amount of formulation investigations that have taken place little information has been provided on the kinetics associated with particle size distributions in these mixtures. This is rather important due to the nature of AP's decomposition pathway. During sublimation AP develops a sponge-like structure (Figure 1), which actually controls the decomposition of AP. If the sample particle morphology changes then the sponge changes, which should lead to different decomposition kinetics. Since the decomposition is regulated via sublimation its behavior should be influenced by pressure, where under elevated pressures, sublimation would be shifted to higher temperatures, which may change the mechanism of decomposition. This is additionally complicated by the reaction of the species adsorbed on the surface, whose porosity increases during the initial stages of decomposition (Figure 1).[1,5,6,7] One of the key influencing factors of solid $\Rightarrow$ gas reactions is the surface area. By changing the particle size from large single crystals down to fine powders, the surface area can easily be modified, thereby changing the initial stages of decomposition.

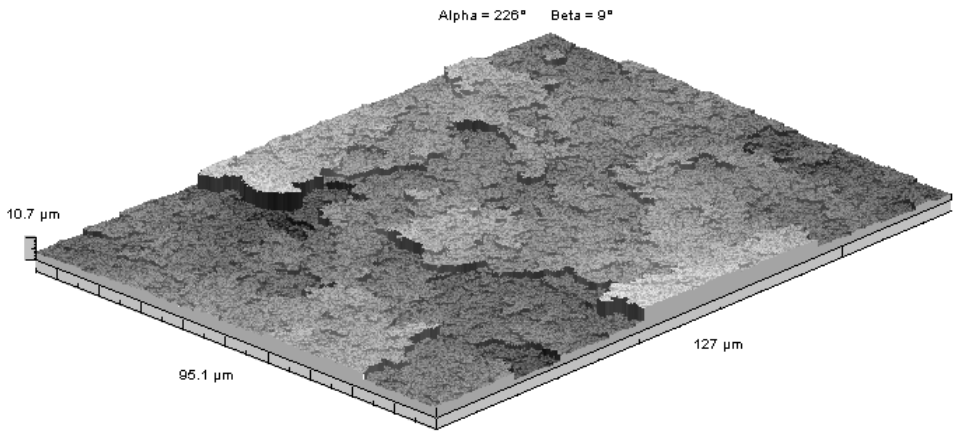

Figure 1. Surface image of the sponge structure developed by AP crystals during the first exothermic mass loss step.

Bircumshaw and Newman performed extensive work on the low temperature (215-275ºC) decomposition behavior of AP, where they tracked changes in the pressure exerted by the decomposition products[8]. They found that depending on the crystal diameter there was a maximum rate associated with an intermediate size of 0.104 - 0.124 mm, where the diameters ranged from 0.18 to 0.051 mm. The effect is quite common for solid – gas decompositions whose rate increases with the number of the surface defects that function as reaction centers. As the crystal size decreases, the surface area increases and so does the number of the reaction centers. The surface area is obviously a key factor in promoting the reaction of adsorbed gases. Decreasing the initial size of the AP crystals should, therefore, result in an increased contribution from the surface reaction. By increasing the pressure under which these experiments are conducted the evolved gases are forced to remain in the sponge structure longer, which should promote the chances of a surface reaction. On the other hand, the use of elevated pressure suppresses sublimation, which slows down adsorption of ammonia and perchloric acid.

The characterization of the sublimation process for AP has been discussed in detail. The experimental activation energy for AP sublimation is typically found to be between one half and one third of the sublimation enthalpy, i.e., in the region 80 – 130 kJ mol^{-1}.[5] However this result is often debated due to the close overlap between sublimation and the surface decomposition reaction. The leading theories presented are that AP sublimation can either proceed via a vaporization model [1,8,9] or by a stepwise sublimation model (Figure 2). In a stepwise sublimation model, the reaction products migrate via successive diffusion from the most strongly bound state to the least strongly bound state, which corresponds to the adsorption on a smooth surface. On the other hand, recent

density functional computations by Politzer and Lane[10] indicate that sublimation may occur via an intermediate complex $H_3N—H—OClO_3$ whose enthalpy is significantly smaller than that of $NH_{3(g)}$ and $HClO_{4(g)}$ so that the activation energy of the process is estimated to be ~130 kJ mol^{-1}. There is still much debate over the decomposition/sublimation kinetics for AP. It should also be noted that the proposed theoretical models do not predict a dependence of the activation energy on the sample type. Due to the overlap of endothermic sublimation and exothermic decomposition it is difficult to determine the kinetics of one process over the other[11], and typically these low temperature kinetic parameters are used in combustion simulations for propellants[12, 13,14,15]. Another interesting topic is the behavior associated with AP when it is compressed into pellets/cylinders of variable density. AP is often compressed during formulation, so it is also important to determine how the compacted system will behave considering the highly variable surface area, which would be formed.

Although AP is the most popular solid energetic material currently employed for propulsion its AP decomposition yields high quantities of chlorinated gases, which are detrimental to the environment. In an effort to move towards cleaner burning fuels, many alternative routes have been explored.[16,17,18,19,20] As a result, AN has regained an interest as its major decomposition products are water and nitrous oxide [18], and it is also easily produced in mass quantities and rather stable to shock.[19,20, 21]

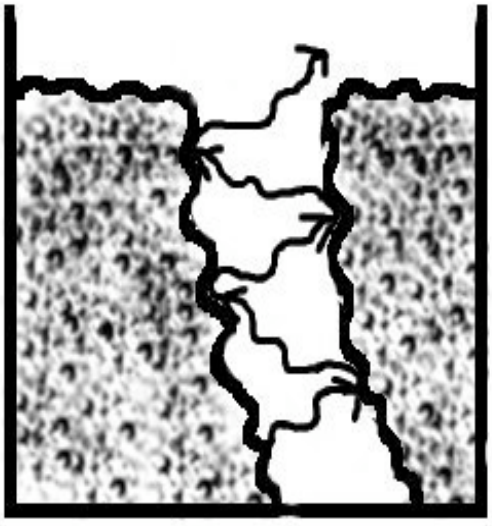

Figure 2. Graphical depiction, showing the progression of sublimated NH_3 and $HClO_4$ gases through the sponge like surface structure of AP

Much like AP, AN's performance is dependent on the way the material is processed. AN decomposition begins around 120°C[4] with a dissociative sublimation step via proton transfer from NH_4^+ to NO_3^- (eq. 4).

$$NH_4NO_{3(s)} \rightarrow NH_{3(g)} + HNO_{3(g)} \rightarrow N_2O_{(g)} + 2H_2O_{(g)} \quad \text{Eq. 4}$$

AN undergoes four solid-solid phase transitions before melting at 169°C[21,22,23,24]. The transitions occur at -17, 32, 84, and 125 °C, the most relevant of which occurs at 32 °C, the ambient temperature region. At this temperature, AN undergoes a phase IV→III transition between two different orthorhombic crystalline lattices. This phase transition is associated with a volume change as well as a significant thermal effect, which is the major drawback to AN. All four transitions, specifically the one at 32°C, present challenges in the application, manufacturing, and storage of AN. The large volume changes can promote cracking in the propellant formulations, which can cause irregular burn properties and damage the propellant housing. In terms of storage, one must also consider the build-up of internal pressure and self-heating within the material. In an attempt to circumvent these problems, a variety of AN formulations have been developed[20]. The problematic volume increase from the phase transition at 32°C has been addressed with phase-stabilized ammonium nitrate (PSAN).[20,25,26,27] This formulation includes a small amount of a metal oxide, such as NiO, into melted AN (Mp ~169°C) and allowed to crystallize. PSAN effectively suppresses the volume changes associated with the IV→III transition by locking the sample in an intermediate phase, preventing the material from converting to phase IV or III. Instead, the material undergoes a phase transition around 50°C to phase II, which has a heat release/absorption

associated with it, but little volume change. This material still has the problem of generation/dissipation of heat, which results from the remaining solid-solid phase transitions[33]. It has been suggested[20] that the most logical way of stabilizing ammonium nitrate would be to separate the NH_4^+ and NO_3^- ions from each other. This, of course, could easily be accomplished, by preparing mixtures of $(NH_4)_3CO_3$ and $Ca(NO_3)_2$. However this would make AN useless as a propellant. Although PSAN improves the utility of AN as an energetic, the majority of AN produced and stored, is in the unstabilized form. In an attempt to increase the energy yields of AN, oftentimes common polymeric fuels or even high explosives[28,29] are added to propellant formulations. The majority of solid propellants consist primarily of an oxidizer, fuel, and polymeric binder (which also serves as a secondary fuel source). Capitalizing on the idea of using polymeric materials as fuels for AN decomposition[33], it would seem that the best approach to the phase stabilization of AN would be to find a way to separate the NH_4^+ and NO_3^- ions from each other within the polymeric fuel[30]. A similar approach is exploited in manufacturing of solid polymer electrolytes (SPE's), where Li^+ salts are co-crystallized with water-soluble polymers such as polyethylene oxide (PEO) (Figure 3). Currently SPE's are widely employed in a variety of areas such as electronics, pharmaceuticals, and agriculture,[31,32,33,34] the most notable applications being time-release drugs, soil nutrients, and rechargeable batteries. These materials require that a strong polar functional group be incorporated into the polymer. Examples of such polymers include polyethylene oxide (PEO), polyacrylamide (PAM), polyvinylpyrrolidone (PVP) polyvinyl alcohol (PVA), etc. Gray[32] has compiled a comprehensive table demonstrating the effectiveness of some common polymer matrices capable of trapping various ions.

The reason such matrices may prove to be useful is that they are environmentally benign, water soluble and very effective in separating ionic compounds and restricting the motion of the ions via polymer transitions such as the glass transition (T_g) or melting.[35,36,37,38]

The physical meaning of the T_g is the onset of the long-range cooperative motion. Below the T_g the polymer chains only experience local mobility so, trapped ions electrostaticly bound to the monomer units, remain separated from each other. Above the T_g, the chain mobility intensifies increasing the probability of an ion interaction, which can lead to a proton or charge transfer (Figure 4). Semi-crystalline polymers such as PEO provide for a different form of isolation as the ions can actually co-crystallize with the polymer matrix. It has been demonstrated that PVP, which has a large dipole moment due to the amide functional group in the pyrrolidone ring, is capable of a strong interaction with cations as reported for Li^+ in a PVP-$LiClO_4$ system[39], where the T_g of the polymer is influenced by the % salt in the matrix. Through application of such systems, it should be possible to prevent AN from existing in a crystalline form, as well as to control the temperature at which the NH_4^+ and NO_3^- come together in the polymer matrix.

The goal of this work is to explore ways of controlling the reactivity of AN and AP through thermal analysis techniques, advanced kinetic studies, and theoretical computations to assist in the optimization of practical applications of energetic formations.

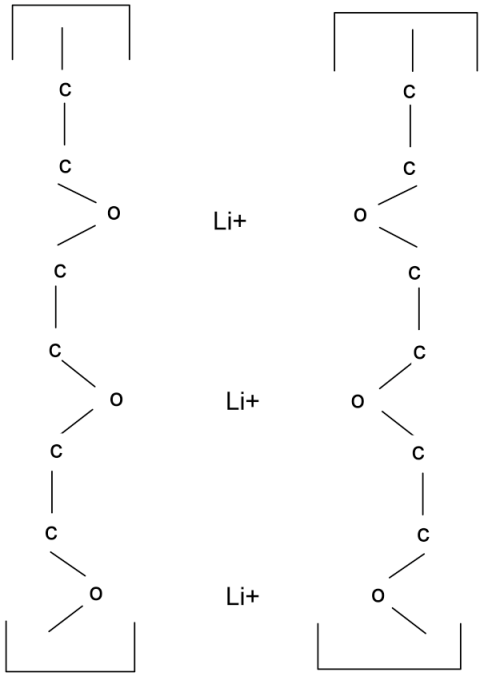

Figure 3. Demonstration of how Lithium ions bind with the water-soluble polymer,PEO.

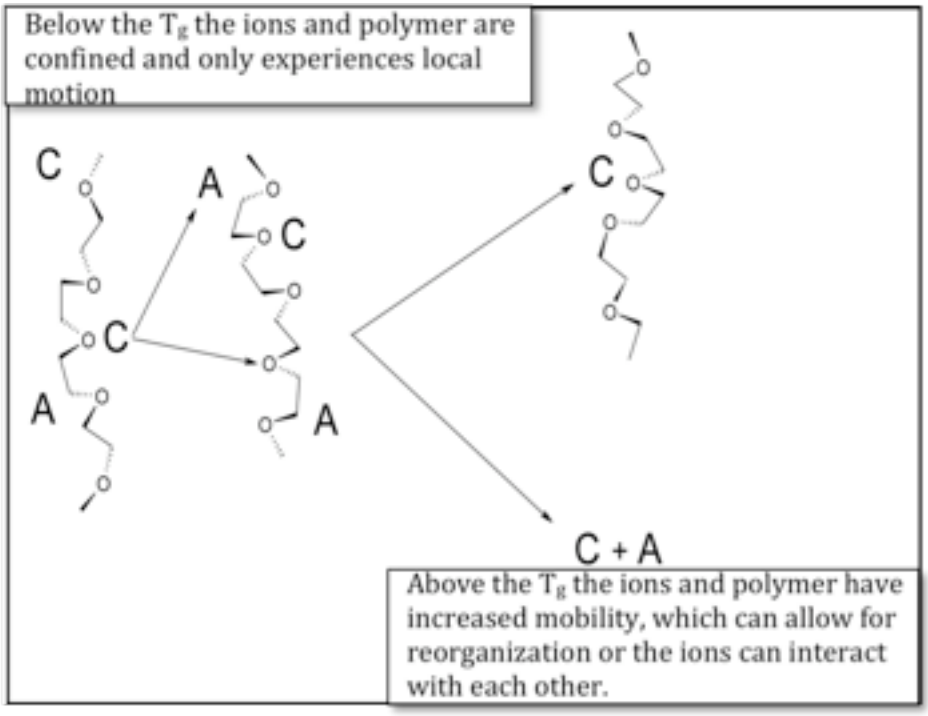

Figure 4. Demonstration of how the anion and cation of salts can orient themselves through the polymer host's mobility restrictions

RESEARCH OVERVIEW: **Techniques Utilized.**

Decomposition kinetics over broad temperature ranges will be tracked, where sublimation, polymer transitions, and decomposition are intertwined. Throughout this work the advanced isoconversional method, developed by Vyazovkin[40,41] will be applied in order to obtain the effective activation energies of the decomposition of AP, PVP-AN and PAM-AN systems. Isoconversional methods have been recognized as an accurate method for the determination of the activation energy for complex processes (ICTAC Kinetic Project)[42]. The method tracks the activation energy changes throughout the entire thermal program/study which allows for a more accurate kinetic assignment of the individual steps of complex reactions which is typically observed in solid state materials[22].

Thermal analysis techniques including Differential Scanning Calorimetry (DSC), Thermogravimetric Analysis (TGA), TGA-Fourier Transform Infrared Spectroscopy (TGA-FTIR), and a heated FTIR sample cell, are employed in these studies. Through the application of DSC; phase transitions (changes in crystalline lattice); endothermic sublimation/vaporization; endothermic degradation; and exothermic decomposition can be observed. DSC is sensitive to solid-solid phase transitions, and will be utilized to verify the presence of crystalline phases in these of materials[43]. DSC can detect changes in solid-solid transitions, which result from additives as in the case of PSAN, where it is important to verify the formation of the stable intermediate phase.[26,16] DSC is often utilized to observe the glass transition of materials. Changes in the T_g of a polymer can occur as a result of additives, mechanical stress, and changes in polymer orientation.

Along with each of these transitions, there is an associated enthalpy, which will be quantified. The temperature and enthalpic data generated can be further examined through the application of kinetic analysis techniques, which can assist in the determination of parameters such as the effective activation energy for solid-state processes. TGA measures mass loss as a function of time and temperature[43]. With the application of the Advanced Isoconversional method the effective activation energy throughout the entire weight-loss process can be determined. TGA-FTIR is a powerful technique in which the off-gassed material from the weight-loss steps is transferred to an FTIR gas cell[44]. With the resulting information, a qualitative assessment of the out-gassed materials can be ascertained which further assists in the understanding of the mass steps. By utilizing a heated FTIR cell to observe the materials as a function of temperature, the bonding of solvents and additives in the host can be tracked through changes in functional group intensities and shifts.

With the application of thermal analysis and solid-state kinetics many of the macro-properties of a material can be ascertained, however, a greater insight at the molecular level is often needed. As a result the application of structural calculations will be applied to these systems. This will primarily be performed by density functional type calculations as these have been shown to yield results which closely match ground state geometries[45,46]. Through these studies a greater knowledge of ion-polymer interactions can be revealed, as well as assist in the prediction of possible reaction pathways during decomposition.

The application of advanced microscopy techniques including hot-stage crossed polarized light microscopy and non-contact optical profilometery, lend further insight

into the thermal behavior of AN and AP based systems. The hot-stage polarized microscope can allow for a visual confirmation of crystalline phases as function of temperature for AN/AP systems. Non-contact optical profilometery collects surface images. This technique can be powerful when examining the different stages of decomposition of AP, especially in the identification and characterization of the sponge structure developed by AP.

THE EFFECT OF PRESSURE AND SAMPLE TYPE ON THE DECOMPOSITION OF AMMONIUM PERCHLORATE

by

ANTHONY J. LANG AND SERGEY VYAZOVKIN

Combustion and Flame; 2000, 145, 779–790

Format adapted and errata corrected for dissertation

ABSTRACT

Differential scanning calorimetry (DSC), thermogravimetric analysis (TGA), and high pressure DSC (HP-DSC) have been used to study the thermal decomposition of ammonium perchlorate samples in the form of 2mm monocrystals, 265μm, and 3μm powders; and pellets pressed to 4 and 7 tons. HP-DSC runs have been performed to determine the effect of pressure on decomposition. TGA and DSC techniques have been employed to examine the effect of sample type on the kinetics of the process. The effects have been evaluated as changes in the temperature, reaction heat, and the rate of decomposition. Isoconversional kinetic analysis has been carried out to detect changes in the effective activation energy of the process. These measurements and calculations show that sublimation and decomposition for ammonium perchlorate to be highly dependent on sample preparation and applied pressure. This calculation identifies the activation energy for the early stages of sublimation/decomposition for all samples start at ~120 $kJmol^{-1}$ which is followed by a dramatic drop to ~60 $kJmol^{-1}$ at 20% mass loss. The activation energy for the later stages of sublimation/decomposition vary with sample type ranging from ~95-145 $kJmol^{-1}$

KEYWORDS

Ammonium perchlorate, Differential scanning calorimetry (DSC), thermogravimetric analysis (TGA), high pressure DSC (HP-DSC), and Isoconversional kinetic analysis

INTRODUCTION

Ammonium perchlorate (AP) as well as other ammonium salts such as ammonium nitrate (AN) and ammonium dinitramide (ADN) are important materials in

rocket propulsion[1]. Decomposition of ammonium salts usually involves dissociative sublimation to ammonia and a respective acid[2].

$$NH_4^+A^-_{(s)} \Leftrightarrow NH_{3(g)} + HA_{(g)} \quad (1)$$

Since the sublimation process is endothermic, the energetic effect is due to an exothermic oxidation of ammonia by the acid. However, the particular pathway of decomposition depends on the nature of the anion. If the anion is thermally unstable it may decompose before the salt undergoes any appreciable sublimation. This is the case of ADN whose decomposition is highly exothermic when the process is performed in open sample holders under a nitrogen stream[3]. Conversely, heating of AN under similar conditions results exclusively in endothermic sublimation[4]. The thermal decomposition of AP presents an intermediate situation. The process demonstrates an overlap of endothermic and exothermic processes that suggests simultaneous occurrence of dissociative sublimation and decomposition[5]. The importance of both processes in the thermal decomposition of AP has been emphasized by Jacobs[6]. The simultaneous occurrence of the two processes complicates the overall kinetics of AP decomposition giving rise to the effective activation energies that vary throughout the process [5]. The process is additionally complicated by the reactions of the species adsorbed on the surface, whose porosity increases during initial stages of decomposition[2,7,8,9.] The surface area of a solid is generally known to be a major parameter affecting the rate of gas-solid reactions. This parameter can be modified by preparing a solid sample in the form of a single crystal, pressed pellet, or a powder. The present paper examines the effect of the sample type on the overall kinetics of the thermal decomposition of AP at slower heating rates. Kinetic information obtained for these conditions is of foremost importance for

hazard evaluations such as under slow cook-off conditions[10]. The lower temperature kinetic parameters are also frequently used in combustion simulations of AP and AP based propellants[11,12,13,14].

EXPERIMENTAL

AP (99.8% purity) was purchased from Aldrich and used without further purification or additives. The as-received AP has an average crystal size of ~265μm. The sample is assigned the name AP265. Large AP crystals (approximately 1.9 mm in diameter) were grown by evaporation of a saturated solution. The sample name is AP1900. AP powders were prepared by grinding in a Fritsch Pulverisette 6 ball mill for 6 hr at 300 RPM's. The ball mill was cleaned three times by milling granulated NaCl under the same program as the AP samples. The resulting crystal size was around 3μm. The sample is denoted AP3. AP pellets were prepared by putting ~0.2g of AP3 powder in a 13 mm die set and pressing it with a hydraulic press. The press loads used were 4 and 7 tons for approximately thirty minutes and the respective sample are denoted AP4T and AP7T. The resulting density of AP7T is ~ 1.85 g cm^{-3} and AP4T is ~ 1.73 g cm^{-3} that is somewhat smaller than the density of an AP crystal (~2.0 g cm^{-3}). The pellets were then cut to the ~ 1.5 mm pieces with a razor blade.

Differential scanning calorimetry (DSC) was employed to measure the heat release of decomposition at ambient and elevated pressure. The respective measurements were taken by using DSC822[e] and DSC27HP, both modules are manufactured by Mettler-Toledo. All integrations were made with a linear base line, which spanned the entire length of the thermal event. Thermogravimetry was used to follow the mass loss kinetics. These measurements were taken on a Mettler-Toledo TGA/SDTA851[e]. AP

samples were studied in 40 μL aluminum pans without lids (one experiment did require a pierced lid on the pan.). All runs were performed on small samples (2-3 mg) in order to minimize self heating-cooling. The DSC and TGA measurements were obtained in a flowing atmosphere of nitrogen gas (purity grade 5.0) at a flow rate 100 ml min^{-1}. The HP-DSC used nitrogen gas to maintain a constant pressure of 0.5 MPa. In all instances nonisothermal programs were employed with a heating cycle from 200 to 550 °C. All measurements were performed in triplicate to verify results. The heating rates used were 2, 5, 7, 9, and 12 °C min^{-1}. Non-contact optical profilometery was performed to take surface images of the AP samples using Fogale Nanotech Microsurf 3D instruments and software.

Kinetic Analysis

In this paper we employ an advanced isoconversional method[15,16] in order to obtain effective activation energies of the decomposition of AP. Isoconversional methods have been recognized as being an accurate way for determining the activation energy of various processes by the ICTAC Kinetic Project[17]. The advanced isoconversional method was developed by Vyazovkin[15,16]. For a series of n experiments carried out under different temperature programs, T_i (t), the activation energy, E_α is determined at any particular extent of reaction, α by finding E_α, which minimizes the function

$$\Phi(E_\alpha) = \sum_{i=1}^{n} \sum_{j \neq i}^{n} \frac{J\left[E_\alpha, T_i(t_\alpha)\right]}{J\left[E_\alpha, T_j(t_\alpha)\right]} \tag{2}$$

where:

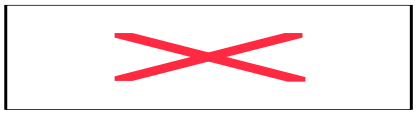

(3)

The method offers two major advantages over the simpler isoconversional methods of Flynn and Wall[18] and Ozawa[19]. The first advantage is that the method has been designed to treat the kinetics that occur under arbitrary variation in temperature, $T(t)$ which allows one to account for self-heating/cooling detectable by the thermal sensor of the instrument. The second advantage is associated with performing integration over small time segments (Eq. 3) that allows for eliminating a systematic error[9] occurring in the Flynn and Wall and Ozawa methods when E_α varies significantly with α. In Eq. 3 α is varied from $\Delta\alpha$ to 1-$\Delta\alpha$ with a step $\Delta\alpha = m^{-1}$, where m is the number of intervals chosen for analysis. The integral, J in Eq. 3 is evaluated numerically by using the trapezoid rule. The minimization procedure is repeated for each value of α to find the dependence E_α on α. As the method tracks the activation energy changes throughout the entire decomposition process, it allows a more accurate kinetic assignment of the individual steps of complex decompositions such as those typically observed for propellants[10]. The extent of conversion α, was determined for DSC data by setting the onset of the thermal event to 0.0α and the end of the thermal event to 1.0 α. From this assumption it is possible to construct E_α dependence on α.

RESULTS

TGA and DSC

The first endothermic peak (240°C) in the DSC scans (Fig. 1) corresponds to the morphological transition from an orthorhombic to a cubic phase of AP. Further heating of AP in open pans is accompanied by an exothermic peak (308°C) followed by an endothermic one[5,6]. As shown earlier[5], the endothermic peak disappears when

decomposition is conducted in pans closed with a pierced lid and an exothermic peak is seen at ~425°C.

The results of the DSC and TGA runs performed on AP of different crystal sizes and sample types are presented in Fig.'s 2, 3, 4, and 5. DSC data (Fig. 2) for the ball milled powder (AP3) sample demonstrate a sharp exothermic peak at 279°C followed by an endothermic event. The grain sample (AP265) shows a similar pattern of decomposition; however the exothermic peak is less intense and occurs at a higher temperature (305°C). The following endothermic event is similar with that observed for AP3. In contrast to the previous two samples, the single crystal (AP1900) did not show obvious signs of exothermic reaction, but an endothermic peak was present.

TGA data (Fig. 3) also show noticeable differences in decomposition of the three samples. Both the ball mill powder (AP3) and the grain samples (AP265), demonstrate a two-step mass loss process. However, in AP3, the first step occurs at ~20%, whereas in AP265 it is about 30%. For the large single crystal (AP1900), the mass loss occurs in a single step and starts at greater temperature than in AP3 and AP265. TGA data (Fig. 4) demonstrates a two-step process for both AP4T and AP7T just as for AP3 and AP265; however, these steps begin and terminate at higher temperatures. From this data it is clear that the less dense pellet (AP4T) starts to lose mass around 275°C whereas the denser pellet (AP7T) mass loss is at 300°C. In both cases the initial mass loss step terminates at ~20% mass loss.

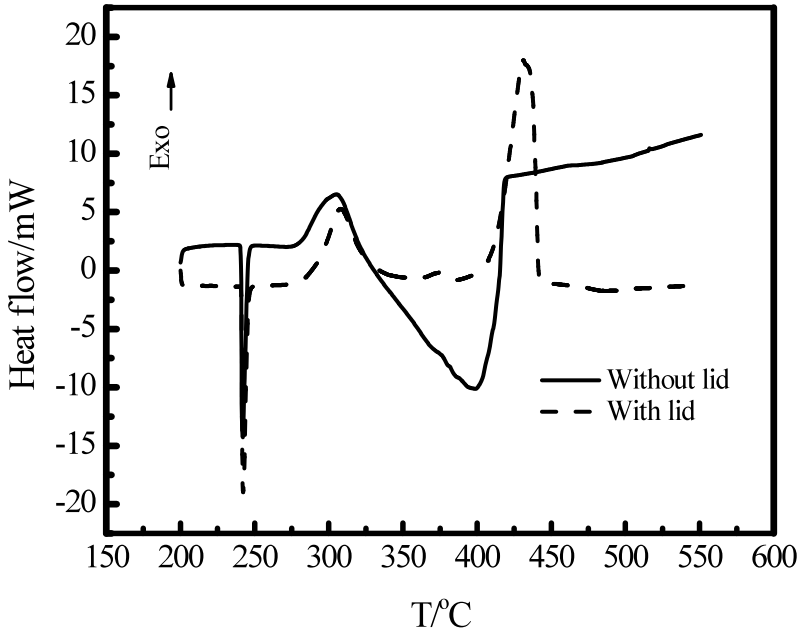

Figure 1. A DSC comparison between AP265 in an open sample holder and a sample holder with a pierced lid at 12°C min^{-1}.

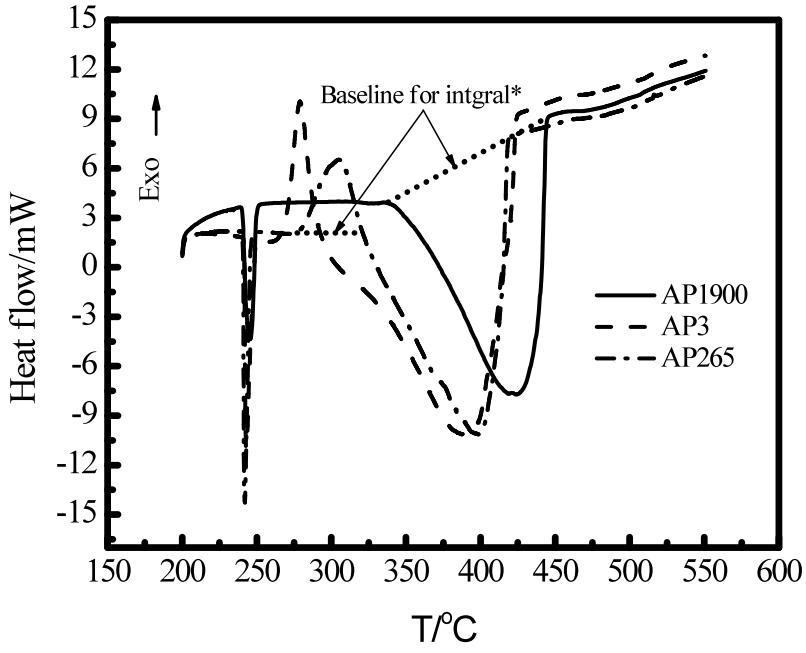

Figure 2. DSC curves identifying the effect of crystal size on the thermal events of AP at 12°C min^{-1}.

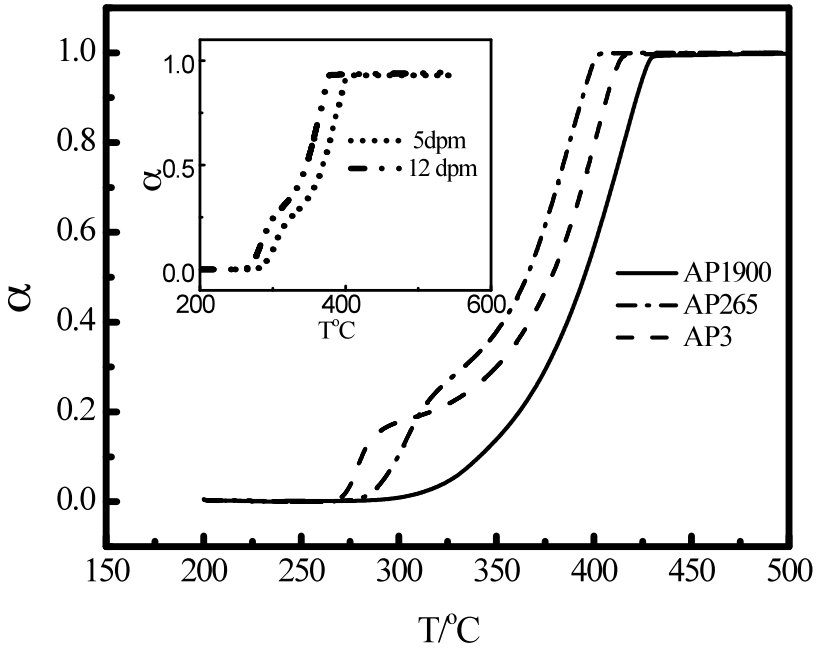

Figure 3. TGA curves comparing various crystal sizes at 12°C min^{-1}. Inset identifies the effect of different heating rates on AP3. (5 and 12 $^{o}C\ min^{-1}$)

It appears that the pellet's thermal behavior approaches that of the single crystal as the density of the pellet increases. The DSC data for these two samples (Fig. 5) reveal thermal events similar to the powders, and the single crystals. The exothermic peak for AP4T occurs around ~320°C and ~340°C for AP7T, which is a shift in exothermic temperature by about 25°C from the powder samples. The endothermic peak terminates at about the same temperature as for the single crystal (AP1900). A unique feature of the pellet experiments is the broadening of the phase transition peak at ~240°C.

The heats associated with the exothermic and endothermic events observed in the DSC during decomposition of AP are given in Table 1. The heats, Q, were determined by calculating the areas of the respective peaks under a heating program of 12°C min^{-1} and using Eq. 4.

$$Q = \left(\frac{q}{m_e}\right)(M)\left(\frac{1}{1000}\right) \tag{4}$$

Here q is the calculated area of the peak in mJ, m_e is the mass loss of the event, and M is the molecular weight of AP. (When the heating program terminates. 0.0 mg of AP remains in the sample container so only the mass loss during the thermal event is used for this calculation.) These values depend greatly on the baseline assumption so great care was utilized to insure that the baseline was the same for all repeated measurements of the same sample type.

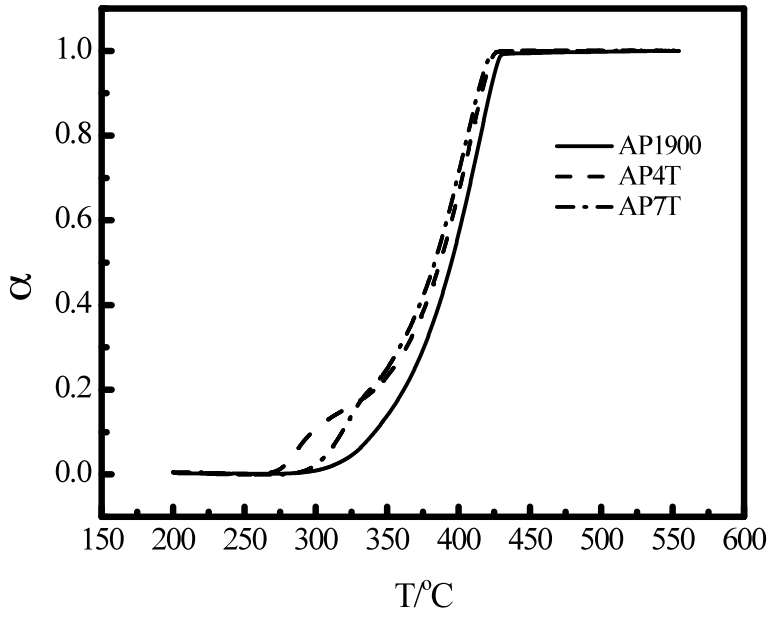

Figure 4. TGA curves comparing pellets of different densities at 12°C min^{-1}.

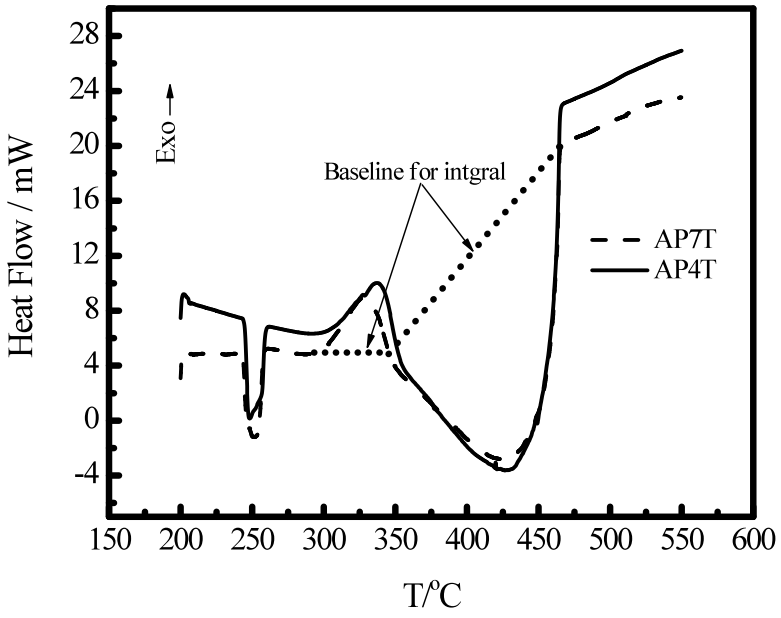

Figure 5. DSC curves of AP pellets at 12°C min^{-1}.

TABLE 1. Heats of exothermic and endothermic processes for the five samples of AP at 12 °C min-1

Sample	Exo-Q / kJ mol^{-1}	Endo-Q / kJ mol^{-1}
AP3	133±4	287±38
AP265	94±14	306±61
AP4T	82±11	226±4
AP7T	78±7	228±29
AP1900		176±17

Identifying the true baseline is difficult so all baselines were constructed the same so as to minimize error. The baseline is configured so that it begins at the onset for a thermal event and terminates at the end of the thermal event. An example of the extrapolated baseline is shown in figures 2 and 5. The TGA data were used to correlate the respective areas with the mass loss that occurred during a particular effect. The relatively large confidence intervals obtained for the endothermic effects are associated with the unavoidable difficulty of selecting a proper baseline for the endothermic peak. It is, however, clear that both of the powders and the pellets demonstrate a markedly larger heat of sublimation than the large crystal sample AP1900. It is also obvious that during the exothermic process AP3 releases noticeably more heat than AP265 which in its turn is greater than that released by the pellets (AP4T, AP7T).

The results of the HP-DSC runs (Fig. 6) for AP3 and AP265 show the initial exothermic decomposition process at approximately the same positions as in the regular DSC measurements (Fig. 2). In HP-DSC runs, AP1900 shows a small exothermic peak at about 350°C (Fig. 6) that was not observed in the regular DSC runs. Upon termination of the initial exothermic peak further heating causes a secondary exothermic event that starts at about 400°C.

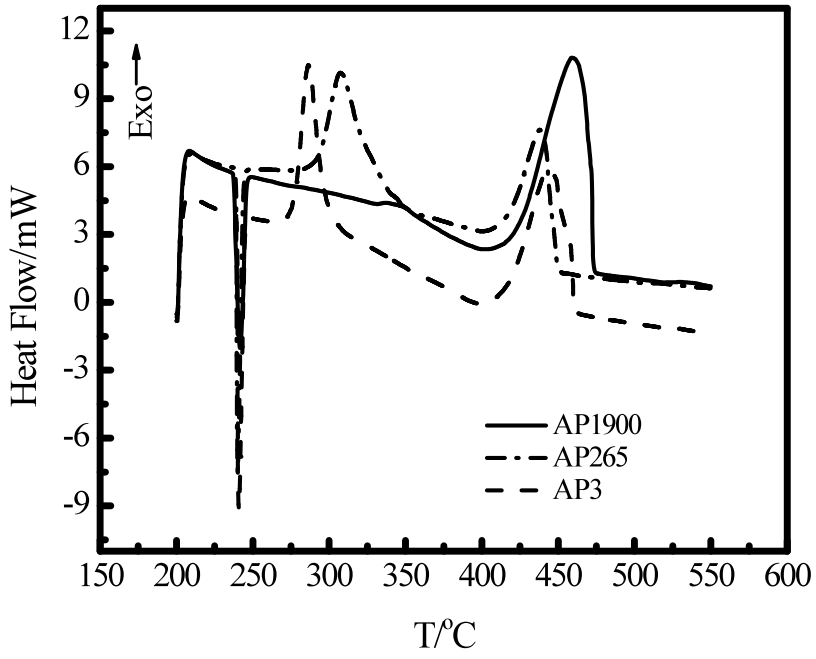

Figure 6. HP-DSC data comparing various crystal sizes at 12°C min^{-1} at 0.5 MPa.

Kinetics

The application of the advanced isoconversional method to the TGA data yielded E_α values that vary with α (Fig.'s 7, 8). In Fig. 7 it is seen that all three E_α values pass through a minimum followed by a plateau. As "α" increases, the initial values of E_α are around 100 – 120 kJ mol^{-1} and quickly drop to 60 – 70 kJ mol^{-1} for all three samples. The major difference is observed in the E_α values related to the plateau. In this region, the respective activation energies demonstrate a noticeable decrease with the decreasing surface area of AP samples.

When the activation energy was calculated for AP4T and AP7T from TGA data it was discovered that both samples demonstrate almost identical activation energy curves. An E_α-dependence for AP4T is shown in Fig. 8. As with the other samples a plateau is observed for the endothermic part of the process that has an activation energy of ~95 kJ mol^{-1}. This activation energy is identical to the value observed for the single crystals (AP1900). The large spike at α ~ 0.2 is a computational artifact due to the intersecting of the TGA curves at this degree of conversion. Unlike all of the other samples, AP4T and AP7T do not show the characteristic decrease in E_α for the early stages of decomposition.

Figures 9-11 were generated via the isoconversional method for DSC data of the three crystals sizes. Figures 10 and 11 show the activation energies for the exothermic reaction which occurs between 300-325°C. Notice that the application of the method to the endothermic peak yields practically constant values of E_α that correlate with the plateau values observed from the TGA data (Fig. 7). The E_α value for AP1900 is ~ 100 kJ mol^{-1} (Fig. 9). For AP265 and AP3, the respective values of E_α are around 110 and 120 kJ mol^{-1} (Fig. 10 and 11).

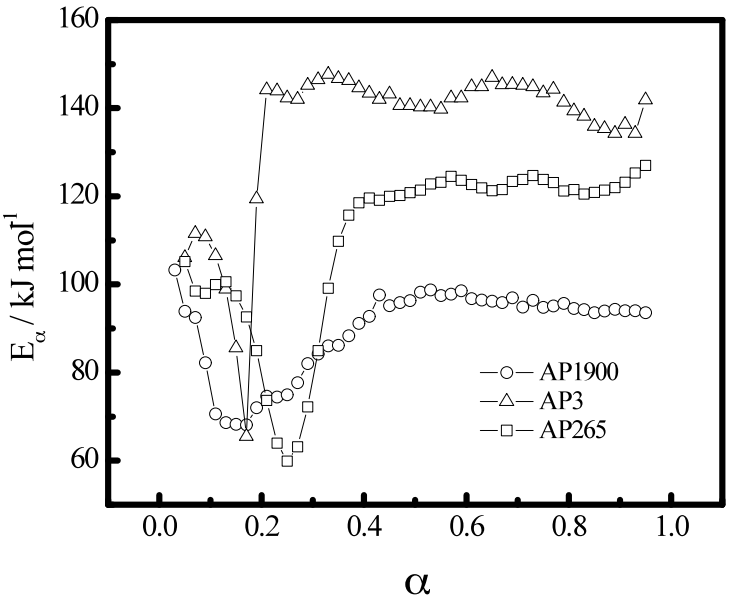

Figure 7. Isoconversional analysis of TGA data for three sample types.

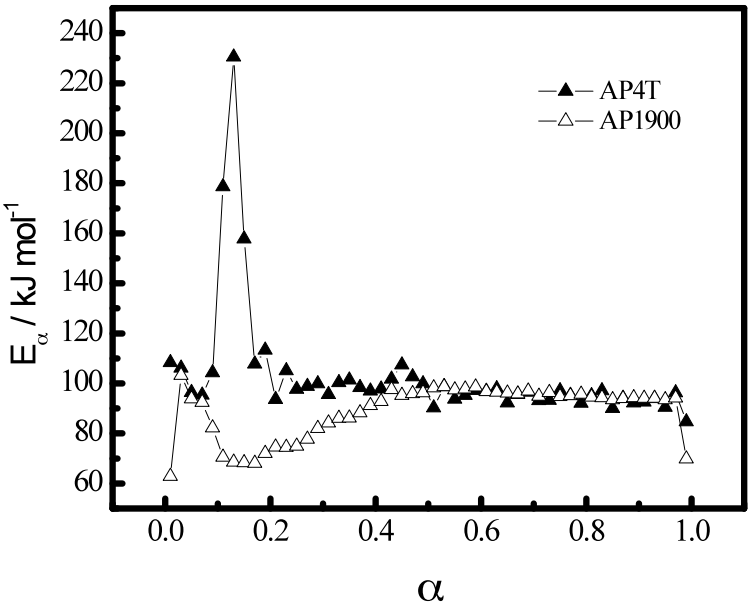

Figure 8. Isoconversional analysis of TGA data for the pressed pellets and single crystals.

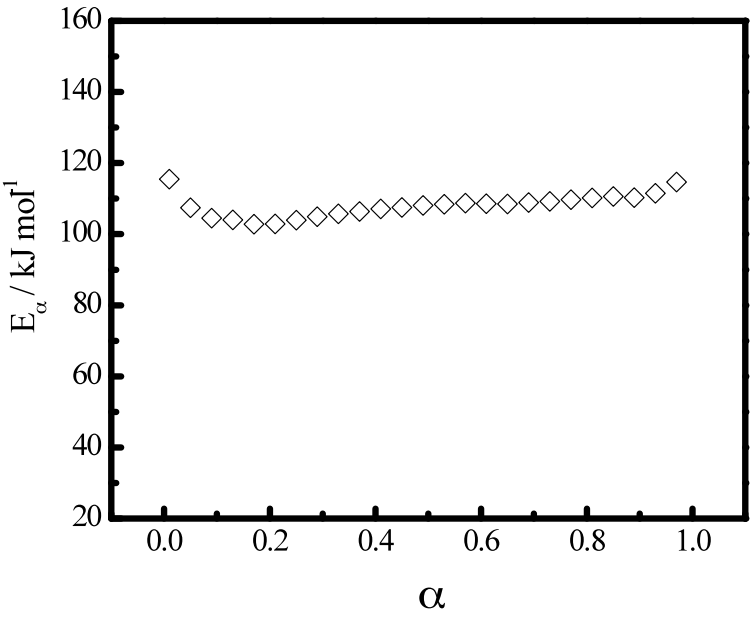

Figure 9. Isoconversional analysis of the endothermic DSC peak of AP1900.

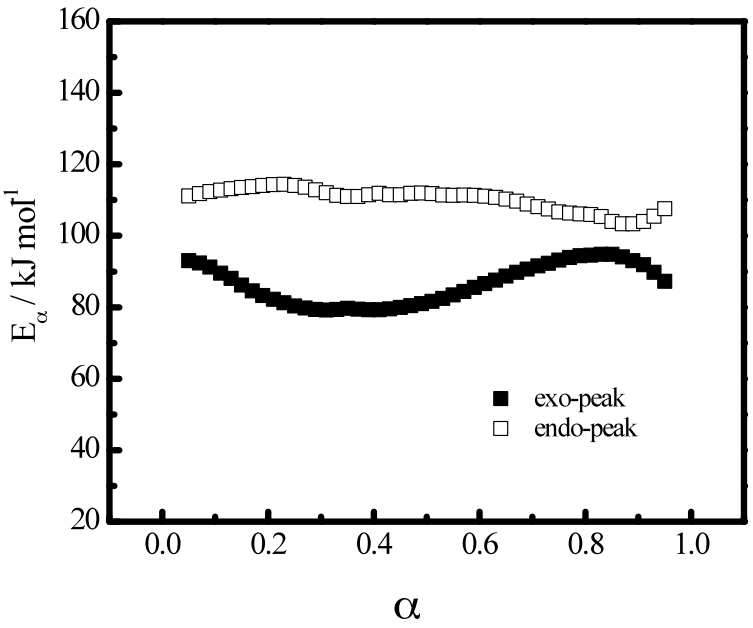

Figure 10. Isoconversional analysis of the exothermic and endothermic DSC peaks of AP265.

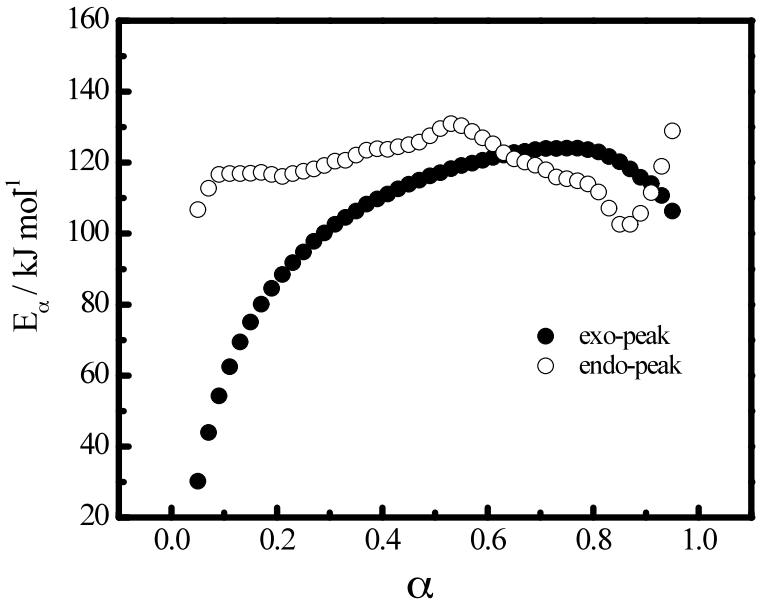

Figure 11. Isoconversional analysis of the exothermic and endothermic DSC peaks of AP3.

In other words, DSC data for endothermic peak show an increase in E_α similar to that observed for TGA at $\alpha > 0.3$ (Fig. 7), although for TGA the effect is more pronounced. It is also noteworthy that the exothermic peak of AP265 gives rise to the E_α dependence that has a shape similar to that obtained from TGA for the early stages of decomposition ($\alpha < 0.4$). The E_α values corresponding to the end of the exothermic peak approach the initial values of the following endothermic peak. A similar feature is observed for AP3 (Fig. 11). Although the E_α values for the exothermic peak of AP3 increase with α, the initial decrease of E_α found for TGA data is not detected.

DISCUSSION

As suggested by Jacobs[6,7], decomposition of AP occurs as a combination of solid-state decomposition, sublimation, and surface reaction of the adsorbed ammonia and perchloric acid. Both TGA and DSC data indicate that the decomposition temperature decreases with the increasing surface area of the AP samples. The effect is quite common for solid – gas decompositions whose rate increases with the number of the surface defects that work as reaction centers. As the crystal sizes decrease, the surface area increases and so does the number of the reaction centers. It is known that during the initial stages of decomposition AP develops a sponge-like structure that has a markedly larger surface area as compared to the virgin crystal (Fig. 12). The surface area is obviously a key factor in promoting the reaction of adsorbed gases. Decreasing the initial size of the AP crystals should, therefore, result in an increasing contribution of the surface reaction in the following order: AP1900, AP7T, AP4T, AP265, AP3. This is supported by the magnitude of the heats of the exothermic effects (Table 1).

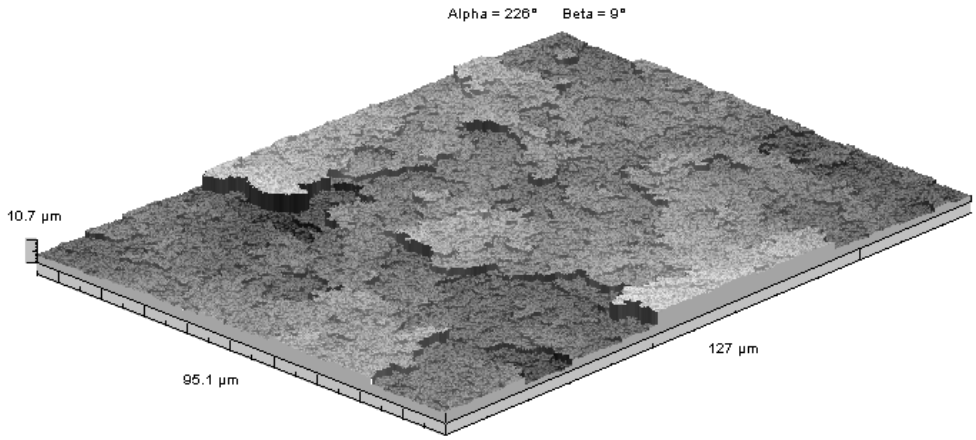

Figure 12. AP1900 at 30% decomposed; Image developed with non-contact optical profilometery.

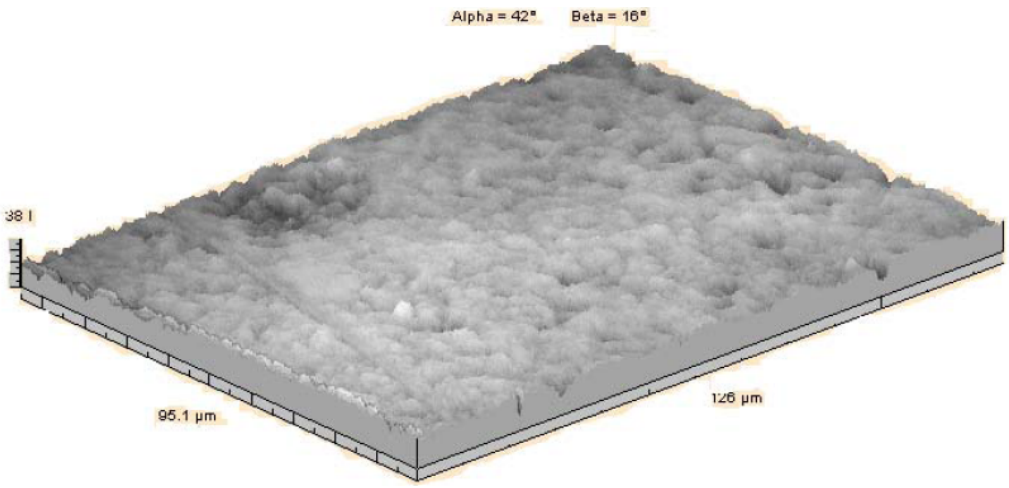

Figure 13. AP7T before decomposition; Image developed with non-contact optical profilometery.

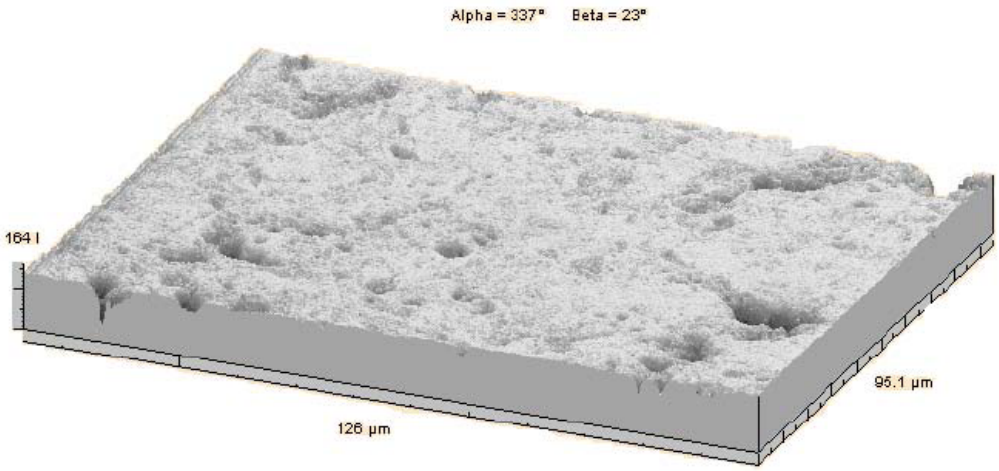

Figure 14. AP7T after 30% decomposition; Image developed with non-contact optical profilometery.

While both pellets (AP4T, AP7T), AP265, and AP3 show a prominent exothermic peak, regular DSC measurements do not detect any exotherms for decomposition of AP1900 in open pans (Fig.'s 2 and 5). However this does not mean that AP1900 does not decompose exothermically at all. In fact, TGA data suggest that AP1900 loses about 12% of its mass by the onset of the endothermic peak. A very weak exothermic peak is detected in AP1900 at ~375 °C (Fig. 6) under elevated pressure. This increase in pressure diminishes desorption of gases increasing the chances of the surface reaction.

On the other hand, the use of elevated pressure suppresses sublimation that slows down adsorption of ammonia and perchloric acid. As a result, the exothermic effects in AP3 and AP265 appear 5-7 °C later (Fig. 6) than under ambient pressure (Fig. 2).

Under ambient pressure, the exothermic events in AP3, AP265, AP4T, and AP7T are immediately followed by endotherms. The amount of consumed heat (Table 1) is comparable, within the uncertainties, to experimentally measured enthalpies of sublimation, 242±8 kJ mol^{-1} [20] which suggests that the late stages of AP decomposition occur predominantly via the sublimation channel. Unexpectedly, the size of the endothermic effect in AP1900 is noticeably smaller than the enthalpy of sublimation, which can be explained by the presence of an exothermic process occurring simultaneously with sublimation. It should be noted that the endothermic peak in AP1900 and the pellets occur about 50°C higher than in AP3 and AP265. For this reason, DSC may detect the exothermic heat of the gas phase reaction of the sublimation products of AP1900, as it occurs at a much faster rate than for AP3, AP265.

Under elevated pressure (Fig. 6) the endothermic peak disappears and an exothermic one arises above 400°C. A similar effect is accomplished in regular DSC runs

when placing a lid on the sample pan (Fig. 1). In both cases the escape of the sublimation products from the reaction zone is hindered so that they can become adsorbed on the AP surface or react in the gas phase, which produces a significant exothermic effect. Note that by the onset of the second exothermic peak, AP265 retains ~64% of the initial mass when the sample is in a pierced pan and under high pressure AP1900 retains ~66% of its initial mass.

The measurements on samples obtained in the regular DSC in a closed sample holder showed two differences from the HP-DSC measurements; the onset temperature of the second exotherm occurs about 15°C lower and appears more intense than in the elevated pressure experiments (Fig. 6). This can be explained by the mass that remains in the sample holder in each case just before the exotherm occurs. In the HP-DSC, ~23% of its initial mass is present at the initial stages of the second decomposition reaction, which is less than half the mass of the sample in the closed pan.

The pellets (AP4T, AP7T) exhibit characteristics of both powders and single crystals. There is one difference associated with the pellets that is not seen in the other samples. It is the broadening of the endotherm at 240°C that is most likely associated with the large stress inside the pellets that slows down the transition to the larger volume cubic phase. The surface features of the pellets before and after 30% decomposition (Fig.'s 13, 14) may provide clues for thermal behavior that is not observed for the single crystal samples. It is seen that sample surface develops large deep holes. This is likely a result of the pellets being more porous than the single crystal. As stated earlier, the specific volume of the pellets is about 10-15% larger than that for the single crystal. Some of the surface pores may serve as nucleation centers for the development of the

holes. The formation of the large holes in addition to the regular sponge like structure observed in the single crystal (Fig. 12) results in the ability to trap the evolved gases more efficiently therefore giving rise to the exothermic decomposition not observed in AP1900.

The kinetic evaluations (Fig.'s 7-11) reveal several pieces of information about the overall reaction. First of all, the TGA and DSC data yield generally consistent kinetic information. Obviously one cannot expect identical results because the two techniques measure different physical properties, and the respective sublimation and decomposition channels are most likely to have differing relative contributions to the heat flow and mass loss. The TGA data appears more reliable as their kinetic analysis does not require any assumptions about the baseline, whose choice may introduce certain systematic errors.

For all five samples, at low conversions E_α is around 100 kJ mol^{-1} which agrees well with the activation energies of nucleation determined by Jacobs and Ng[7]. As the extent of conversion rises to 0.2 – 0.3, the effective activation energy falls down to ~60 kJ mol^{-1} for AP3, AP265, and AP1900. As noted earlier, AP decomposition in that region is associated with the surface reaction. The low value of E_α (~60 kJ mol^{-1}) can apparently be related to the activation energy of the adsorption-desorption process. After E_α for AP3, AP265, and AP1900 passes through the minimum, it rises back to greater values in the plateau region. It should be noted that the plateau values are reached most quickly by AP3 (at $\alpha > 0.2$), which has the largest initial surface area, compared to AP265 (at $\alpha > 0.4$) and AP1900 (at $\alpha > 0.5$) whose initial surfaces areas are much smaller. It appears that the variation of E_α in the pre-plateau region is mostly determined by the evolution of the sponge-like structure in AP. It has been demonstrated[21] that the

surface area of the sponge-like structures formed at decomposition passes through a maximum. The smaller the crystal size (i.e., the larger initial surface area) the faster the structure develops and the maximum is reached. Obviously, the maximum in the surface area of the sponge should be associated with the greatest adsorption capacity and, thus, with maximum contribution of the surface reaction. The pellets (AP4T, AP7T) do not demonstrate the characteristic dip in E_α for the initial exothermic part of the process. The activation energy remains almost constant at ~100 kJ mol^{-1}, suggesting that the process is limited by a single step, which is different from that observed in other samples. It is noteworthy that the E_α value is consistent with the activation energy of AP nucleation. This may indicate that in the compressed samples nucleation is the step that controls the development of the surface area. Recall that unlike single crystals, the pellet samples form holes (Fig. 13). As this is a unique feature of the pellet samples, it does not seem unreasonable to assume that the constant E_α value for at the early decomposition is linked to the development of a porous structure .

As the surface area of the sponge passes through its maximum and starts to decrease, the contribution of the exothermic surface reaction decreases, giving way to the endothermic process of sublimation. This process is represented by the plateau at the later stages of AP decomposition. It is rather unexpected that the effective activation energy of the sublimation process depends on the sample types; ~ 95 kJ mol^{-1} for AP1900 and the pellets (AP4T, AP7T); ~125 kJ mol^{-1} for AP265; and ~145 kJ mol^{-1} for AP3. All these values are significantly smaller than the experimentally determined sublimation enthalpy 242 ± 8 kJ mol^{-1} [20]. It should be stressed that the activation energies for AP sublimation are typically found to be between one half and one third of the sublimation enthalpy, i.e.,

in the region 80 – 130 kJ mol^{-1} 5. Several theories have been advanced to explain the effect. Jacobs and Russell-Jones[7] proposed a model which assumes that the process is controlled by diffusion which gives rise to a theoretical activation energy equal to one half of the sublimation enthalpy. The theoretical value is consistent with their experimental activation energy. Guirao and Williams[22] and Pai Verneker et al[23] have challenged experimental measurements of Jacobs and Russell-Jones and suggested[7] that their data might have been affected by decomposition, which occurs with a higher activation energy. In trying to reproduce the experimental conditions of the study of Jacobs and Russell-Jones, Pai Verniker et al[23] have claimed that the former observed decomposition instead of sublimation. The value they obtained for sublimation in vacuum was around 80 kJ mol^{-1}, which has been found consistent with the Schultz-Dekker model of vaporization [24]. Alternatively, Aleksandrov and Khairetdinov[25] suggest that the E_α equals one third of the sublimation enthalpy and can be explained by the Volmer model of stepwise sublimation, according to which sublimation of the reaction products occurs as a successive diffusion from the most strongly bound state to the least strongly bound state, which corresponds to the adsorption on a smooth surface. On the other hand, recent density functional computations by Politzer and Lane[26] indicate that sublimation may occur via an intermediate complex H3N—H—OClO3 whose enthalpy is significantly smaller than that of NH3 and HClO4 so that the activation energy of the process is estimated to be ~130 kJ mol^{-1}. This means that the E_α around one half the sublimation enthalpy can be explained theoretically without invoking decomposition. It should be noted that the proposed theoretical models do not predict a dependence of the activation energy on the sample type, which was observed in the present study.

We do not think that the larger values of E_α for sublimation of AP265 and AP3 can be explained by the overlap with decomposition, because the observed endothermic effects (Table 1) appear too large to indicate any significant presence of the exothermic decomposition. A contribution from decomposition cannot be ruled out for large crystals (AP1900), for which the observed endothermic effect is noticeably smaller than the sublimation enthalpy (242 ± 8 kJ mol^{-1}). However AP1900, demonstrates the smallest activation energy comparable to the values obtained for sublimation in vacuum. In other words, invoking decomposition would not explain the variation of the activation energy of sublimation with the sample type. Perhaps, the explanation should be sought in changing the conditions of the surface diffusion with the surface area.

CONCLUSIONS

Decomposition of solid AP occurs via two major channels, which include an endothermic sublimation and the exothermic surface reaction of sublimation products. The exothermic process prevails at the initial stages and is associated with the development of a high surface area sponge-like structure in the AP samples. This stage can be enhanced by using fine powders of a high surface area or suppressed by using compressed pellets and single crystal samples. Later stages of decomposition are endothermic under ambient pressure, but can be turned exothermic at elevated pressures or in closed pans. Isoconversional kinetic analysis shows that the initial stages of decomposition demonstrate rather similar kinetics characterized by a change in the effective activation energy from ~100 to ~60 kJ mol^{-1}. This behavior holds for all sample types, but pressed pellets. The latter demonstrate a practically constant value ~100 kJ mol^{-1}. The later stages of decomposition process are associated with sublimation that is

represented by a practically constant activation energy, whose value depends on the sample type. It increases markedly with increasing the surface area from ~95 kJ mol^{-1} for the single crystal and pressed pellets to ~ 145 kJ mol^{-1} for the fine powder.

ACKNOWLEDGEMENTS

Thanks are due to Dr. Andrei Stanishevsky for the photographs of AP and to Mettler-Toledo, Inc for the donation of the TGA instrument used in this work. Partial support for this work came from the Army Research Office under grant DAAD19-02-1-0190 and is gratefully acknowledged.

REFERENCES

1. Kubota, N.; Propellants and Explosives, Wiley-VCH GmbH, Weinheim, 2002.

2. Galwey. A.K.; Brown, M.E.; Thermal Decomposition of Ionic Solids, Elsevier, Amsterdam, 1999.

3. Vyazovkin, S.; Wight, C.A. *J. Phys. Chem*. A **1997,** 101, 31, 5653-5658.

4. Vyazovkin, S.; Clawson, J.S.; Wight, C.A. *Chem. Mater.* **2001,** 13, 960-966.

5. Vyazovkin, S.; Wight, C.A.; *J. Chem. Mater.* **1999,** 11, 3386-3393.

6. Jacobs, P.W.M.; Russell, J.A. *J. Phys. Chem.* **1968,** 72, 202.

7. Jacobs, P.W.M.; Ng, W.L. *J. Solid State. Chem.* **1974**, 9,315.

8. Chang, F.M. Huang, C.C.; Yeh, T.F.; Liu, C.S.; Leu, A.L. *Propellants, Explosives, Pyrotechnics* **1990,** 15, 261.

9. Manelis, G.B.; Nazin, G.M.; Rubtsov, Y.I.; Strunin,V.A. Thermal Decomposition and Combustion of Explosives and Propellants, Taylor & Francis, London, 2003.

10. Brill, T. B.; Beckstead, M. C.; Flanagan, J. E.; Lin, M. C.; Litzinger, T. A.; Waesche, R. H. W.; Wight, C. A. *J. Propul. Power* **2002,** 18, 824.

11. Waesche,R. H. W.; Wenograd, J. *Combust. Expl. Shock Waves* **2000,** 36, 125.

12. Zhou, X.; Jackson, T. L.; Buckmaster, J.; *Combust. Flame* **2003**, 133, 157.

13. Knott, G. M.; Brewster, M. Q. Combust. *Sci. Tech.* **2002,** 174, 81.

14. Panyam,R. R.; Price, E.W.; Chakravarthy, S.R.; *Combust. Flame* **2004,** 136, 1-15.

15. Vyazovkin, S. *J. Comput. Chem*. **1997,** 18, 393.

16. Vyazovkin, S. *J. Comput. Chem*. **2001,** 22, 178.

17. Brown, M.E.; Maciejewski, M.; Vyazovkin, S.; Nomen, R.; Sempere, J.; Burnham, A.; Opfermann, J.; Strey, R.; Anderson, H. L.; Kemmler, A.; Keuleers, R.; Janssens, J.; Desseyn, H. O.; Li, C.R.; Tang, T.B.; Roduit, B.; Malek J.; Mitsuhashi, T. *Thermochim. Acta* **2000,** 355, 1-2, 125.

18. Flynn, H.; Wall, L.A. *J. Res. Nat. Bur. Standards: A* **1966,** 70, 487.

19. Ozawa, T. *Bull. Chem. Soc. Japan* **1965,** 38, 1881.

20. Inami, H.S.; Rosser, W.A.; Wise, H. *J. Phys. Chem.* **1963,** 67, 1077.

21. Simons, J. *J. Phys. Chem. B* **1999,** 103, 8650-8656.

22. Guirao, C.; Williams, F.A. *J. Phys. Chem.* **1969,** 73, 4302.

23 Pai Verneker, V.R.; McCarty, M.; Maycock, J.N. *Thermochim. Acta* **1971,** 3, 37.

24. Schultz, R.D.; Dekker, A.O.; *J. Phys. Chem.* **1956,** 60, 1095.

25. Alexandrov, V.V.; Khairetdinov, E. F. *Kinet Katal* **1971,** 12, 1327.

26. Politzer, P.; Lane, P.J. *Mol. Str. (Theochem)* **1998,** 454, 229.

PHASE AND THERMAL STABILIZATION OF AMMONIUM NITRATE IN THE FORM OF PVP-AN GLASS

by

ANTHONY LANG AND SERGEY VYAZOVKIN

Materials Letters 2008, 62, 1757–1760

Format adapted and errata corrected for dissertation

ABSTRACT

In order to accomplish both phase and thermal stabilization of ammonium nitrate (AN), a new material has been developed, polyvinylpyrrolidone (PVP) - AN glass. PVP is capable of separating AN into its ions through an ion-dipole interaction with PVP. The ions remain separated below the glass transition temperature (T_g) of PVP (~160°C) which is confirmed by the disappearance of the solid-solid phase transitions associated with AN. Above the T_g, AN ions recombine, giving rise to a fast exothermic reaction. The material has been characterized by DSC, TGA, FTIR and quantum mechanical methods.

Keywords: Energetic materials, Composite materials, Polymers, Thermal properties

INTRODUCTION

Ammonium nitrate (AN) is a well-known energetic material widely used as an oxidizer in explosives and propellants. AN undergoes four solid-solid phase transitions before melting at 169°C[1,2,3,4]. The most relevant of which occurs at 32 °C, i.e., in the ambient temperature region. At this temperature, AN undergoes a phase IV→III transition between two different orthorhombic crystalline lattices. This phase transition is associated with a drastic volume change as well as a significant thermal effect, which is the major drawback of the material. In attempt to circumvent these problems, a variety of mixed AN formulations have been developed[5]. However these formulations are usually ineffective in preventing detonations when AN is stored in large quantities. In particular, the problems associated with the phase transition at 32°C have been addressed by developing phase stabilized AN (PSAN)[5,6,7,8]. This formulation includes a small amount of metal oxides such as NiO. The PSAN materials effectively suppress the volume

changes associated with the IV→III transition. Nevertheless, the material still has the problem of generation and dissipation of heat which results from the remaining solid-solid phase transitions[8]. It has been suggested[5] that the most logical way of stabilizing ammonium nitrate would be to separate the NH_4^+ and NO_3^- ions from each other. This, of course, could be accomplished by preparing mixtures of $(NH_4)_3CO_3$ and $Ca(NO_3)_2$ [5]. However this would make AN useless for the propellant industry.

The majority of solid propellants consist primarily of an oxidizer, fuel, and polymeric binder (which also serves as a secondary fuel source). Capitalizing on the idea of using polymeric materials as fuels for AN decomposition[8], it would seem that the best approach to the phase stabilization of AN would be to find a way to separate the NH_4^+ and NO_3^- ions from each other within a polymeric fuel[9]. A similar approach is exploited in manufacturing solid polymer electrolytes (SPE's). Currently SPE's are widely employed in a variety of areas such as electronics, pharmaceutics, agriculture, etc[10,11,12,13]. These materials require a strong polar functional group be incorporated into the polymer backbone. Examples of such polymers include polyethylene oxide, polyacrylamide, polyvinylpyrrolidone (PVP), etc. Gray[11] has compiled a comprehensive table demonstrating the effectiveness of some common polymer matrices to solvate various ions based on hard-soft acid-base interactions for common cations and anions. The reason such matrices may prove to be useful for the current project is that they are environmentally benign, water soluble and very effective in separating ionic compounds and restricting the motion of the ions below the glass transition temperature, T_g of the polymer matrix[14,15,16,17].

In the present paper, we explore the opportunity of AN phase stabilization by introducing AN in a PVP matrix (PVP's structure can be seen in Figure 1). The monomer unit of PVP has a very large dipole moment due to the amide functional group in the pyrrolidone ring, which is capable of a strong interaction with cations as reported for Li^+ in a PVP-$LiClO_4$ system[18].

EXPERIMENTAL

AN of 99.9% purity and PVP (average Mw 1.3 million) were purchased from Acros Organics. AN-PVP mixtures were prepared based on the following mass fractions of 5, 10, 20, 25, 30, 40, and 50% of AN. Films were produced from the solid PVP-AN mixtures by dissolving ~0.5 g of a mixture in 10 ml of methanol. The solutions were poured into aluminum pans and dried under vacuum for 12 hr. The final thickness of the films was ~ 0.5 mm. A differential scanning calorimeter (DSC 822^e) and a thermogravimetric analyzer (TGA/SDTA 851^e) manufactured by Mettler-Toledo were utilized to follow thermal events occurring on heating of the obtained materials. The heating rate in all experiments was 5 °Cmin^{-1}. Fourier transform infrared spectroscopy (FTIR) was employed to record condensed phase spectra of the AN-PVP material at various temperatures.

Computational methods were used to determine the likely positions of the nitrate and ammonium ions in the PVP matrix. Because computational methods scale considerably with respect to the number of atoms (N), PVP was represented by using a single monomer unit. To get a starting idea of the most probable locations of the ions, an electrostatic potential map was generated for the monomer. With an idea of where the ions might be located, optimizations were carried out with parallel quantum solutions

(PQS) software [19]. The initial optimizations were done at the B3LYP/6-31G(d) level of theory. Becke's three-parameter hybrid exchange functional[20] with the Lee-Yang-Parr gradient corrected correlation functional[21] was chosen because it is known to be very accurate for calculating ground state geometries[22]. If more than one minimum was found, the energies of each geometry were compared to determine which is more stable. Once the most stable geometry was found, the molecule was optimized with Dunning's triple-ζ basis set - cc-pVTZ[23] starting from the B3LYP/6-31G(d) geometry. This methodology was carried out for the following: PVP monomer with the nitrate ion, PVP monomer with the ammonium ion, and PVP monomer with the ammonium and nitrate ions. Frequency calculations were then carried out on the optimized structures. These calculations were done at B3LYP/cc-pVTZ//B3LYP/cc-pVTZ with Gaussian 98[24].

RESULTS

DSC Results

Figure 1 displays DSC traces that identify the thermal events in neat PVP and AN as well as PVP-AN films containing different AN concentrations. Neat PVP undergoes the glass transition at around 160°C. Neat AN demonstrates three endotherms due to the solid-solid phase transitions followed by the melting peak. Note that none of these peaks are detected in the AN-PVP films containing 20% of AN. Instead, we observe the large exotherm that develops around the glass transition temperature of PVP. The exotherm increases in size and sharpens as the load of AN is increased. However once the content of AN reaches 40%, DSC starts detecting the phase transitions of AN in the AN-PVP material. The appearance of the transitions suggests that a part of the 40% AN load is present as a crystalline phase. The latter is obviously not present in the AN-PVP material

containing 20% of AN so that this material is a single phase amorphous glass. That is, the maximum load of AN that can be present in the single phase AN-PVP glass is between 20% and 40%.

TGA Results

Figure 2 demonstrates a set of TGA curves of PVP-AN glasses. One can clearly see a drop in mass in the temperature region from 50°C to 125°C for all samples which is a result of water loss as confirmed by FTIR spectra. More importantly, in each case there is a dramatic drop in mass around 160°C that correlates with the glass transition in neat PVP (Figure 1). Note that this mass loss is practically equal to the amount of AN added to the film. This suggest that almost all of the AN that was present in the AN-PVP glass is out-gassing from the PVP matrix at T_g.

FTIR Results

FTIR was employed to detect an interaction between the NH_4^+ ion and the carbonyl of PVP. The spectra of the carbonyl stretching vibration were taken for both a neat PVP sample and an AN-PVP glass at 105°C. In neat PVP, the carbonyl stretch is found at 1650 cm^{-1}. AN-PVP material shows a peak at ~1680 cm^{-1} with a shoulder at ~1650 cm^{-1}. The shift of the carbonyl stretch absorption to higher frequency is consistent with the idea of an ion-dipole interaction between the carbonyl group and NH_4^+. On the other hand, the shoulder is located at practically the same frequency as the carbonyl absorption band in pure PVP (1650 cm^{-1}), which apparently represents unbound carbonyl stretching. These data suggest that the majority, but not all, of the carbonyl groups take part in binding NH_4^+ ions.

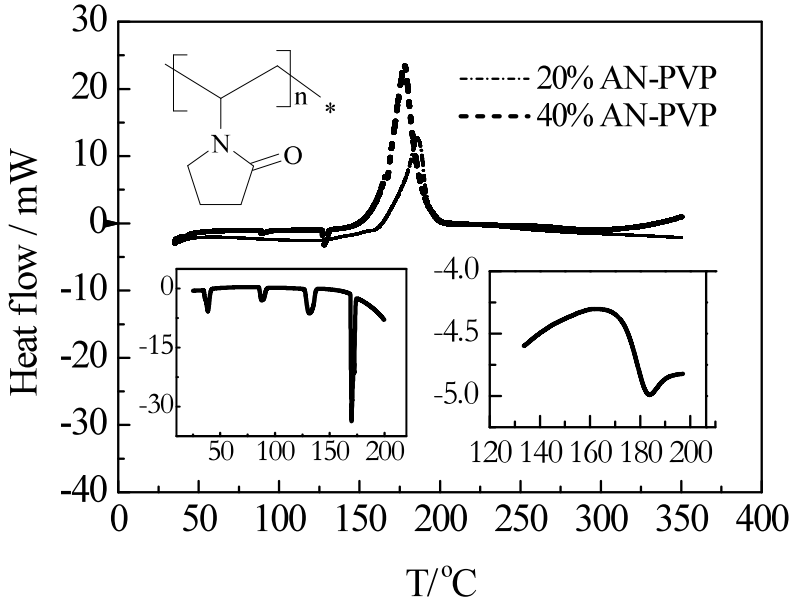

Figure 1. DSC traces for the composite material containing 20 and 40% of AN. (Left Inset: shows AN's phase transitions, Right Inset: shows a step change in the heat flow representing the glass transition in neat PVP.) Exothermic direction is up.

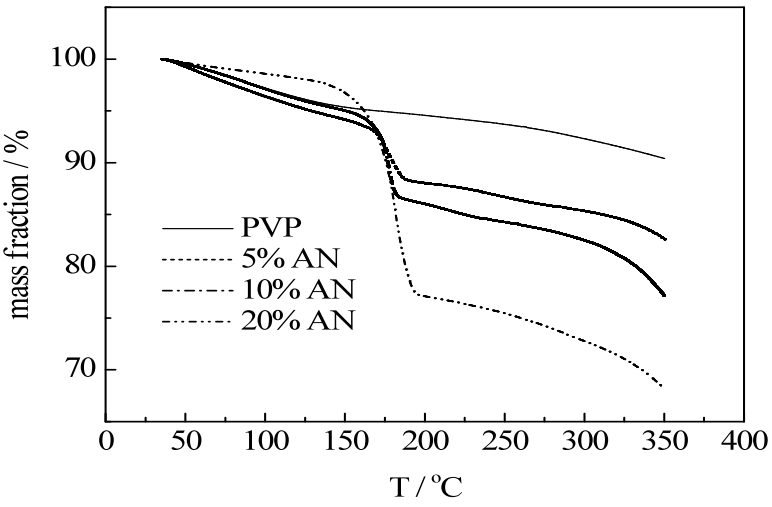

Figure 2. TGA curves for neat PVP and AN-PVP glasses of different AN load.

Calculations

The optimized structures for the PVP monomer unit respectively associated with NH_4^+ and NO_3^- ions is shown in Figure 3. It is seen that the ammonium ion interacts directly with the carbonyl oxygen and nitrate ion centers itself above the pyrrolidone ring to maximize the proton - NO_3^- interaction. The frequency calculations reveal that our optimized structures are indeed minima by the absence of any imaginary frequencies.

DISCUSSION

It is important to emphasize at least two aspects of the present study. First, the DSC data indicates that AN-PVP glass contains a crystalline AN phase at the AN loads above 20%. Since MW of one PVP monomer unit is 111 g mol^{-1} and AN is 80 g mol^{-1}, a 1:1 mole ratio corresponds to ~ 42% mass load of AN. Therefore the separation of NH_4^+ and NO_3^- in PVP requires more than one monomer unit of PVP per AN molecule. The 2 PVP to 1 AN mole ratio corresponds to ~27% mass load of AN that correlates with the load above which the material stops being a single amorphous phase. Because the separation of the AN ions requires at least two pyrrolidone rings, it is reasonable to assume that NH_4^+ and NO_3^- position themselves at different rings.

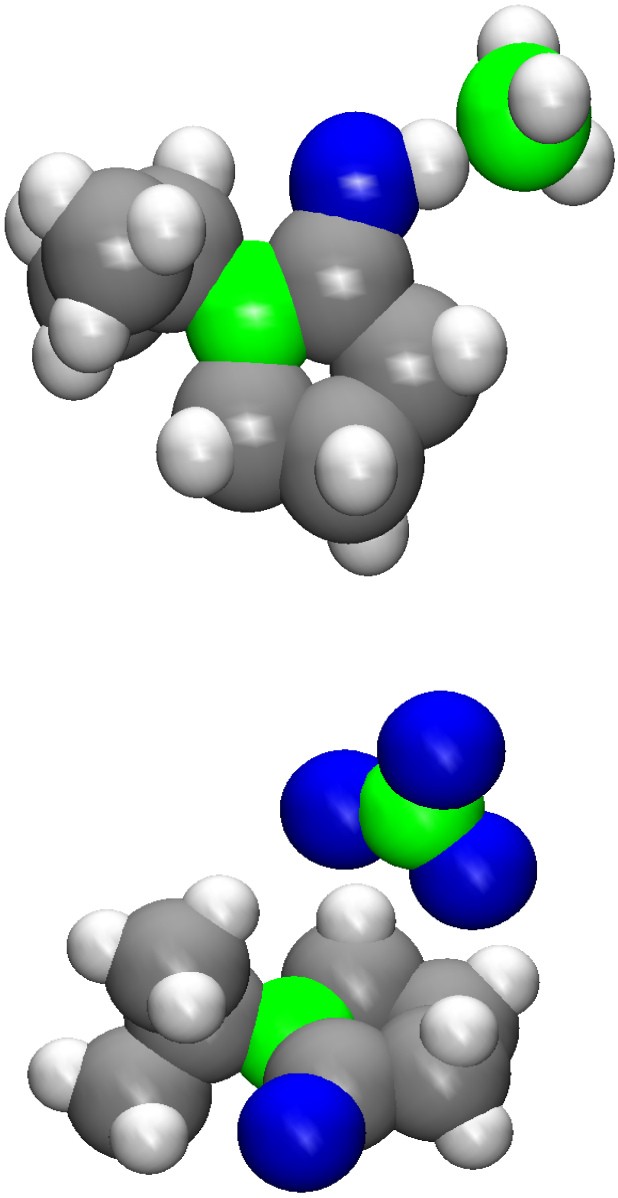

Figure 3. Computational prediction of the most probable binding site for NH_4^+(left) and NO_3^- (Right).

The second aspect is that the appearance of the major mass loss and the exotherm correlate with the glass transition in the PVP matrix. It should be stressed that the glass transition temperature represents the onset temperature of the long range cooperative motion of polymer chains. Below this temperature the polymer chains of the PVP matrix experience only local short range mobility so that the NH_4^+ and NO_3^- ions, electrostaticly attached to the PVP monomer units, can remain separated from each other. However, above T_g the polymer chain mobility intensifies to such extent that the ions can interact with each other. As a result, proton transfer followed by the formation of ammonia and nitric acid becomes possible. It is not surprising that the mass loss and the heat release events (Figure 1 and 2) correlate with the glass transition. Note that the onset of the thermal decomposition of neat AN is around 120°C[25] so that using polymer matrices of higher T_g also provides an opportunity for the thermal stabilization of AN.

CONCLUSIONS

It has been demonstrated that PVP can be used as a matrix capable of separating AN into its ions up to AN loads of ~30% by mass. The separation results from the ion-dipole interaction between the carbonyl group of PVP and the ammonium ion as shown by FTIR measurements. The absence of AN as an individual phase is confirmed by DSC. The resulting material remains a single phase amorphous glass up to the temperature corresponding to the glass transition of the PVP matrix. Above this temperature the material quickly releases gaseous products in amounts practically equal to the mass load of AN. The use of highly polar polymer matrices provides a novel approach to the problem of the phase and thermal stabilization of AN and, possibly, other ionic energetic materials.

REFERENCES

1. Kubota, N.; Propellants and Explosives, Wiley-VCH GmbH, Weinheim, 2002.

2. Turcotte, R.; Lightfoot, P.D.; Fouchard, R.; Jones, D.E.G. *J. Hazard. Mater.* **2003**; a101, *1-27*.

3. Singh, G.; Felix, S.P. *Combust. Flame* **2003**, 135, 145-150.

4. Oommen, C.; Jain, S.R. *J. Therm. Anal.* **1999**, 55, 903-918.

5. Oxley, J.C.; Smith, J.L.; Rogers, E.; Ming, Y. *Thermochim. Acta*, **2002**, 384, 23-45.

6. Simoes, P.N.; Pedroso, L.M.; Portugal, A.A.; Campos, J.L. *Thermochimica Acta* **2000**, 364,71-85.

7. Mathew, S.; Krishnan, K.; Ninan, K.N. *Propellants Explos., Pyrotech.* **1998**, 23,150-154.

8. Carvalheira, P.; Gadiot, G.M.H.J.L.; de Clerk, W.P.C. *Thermochim. Acta* **1995**, 269/270, 273-293.

9. Abthagir, P.S.; Saraswathi, R. *Mater. Chem. Phys.* **2005**; 92: 21-26.

10. Meltzer, Y.L. Water-Soluble Polymers: Developments Since 1978, Noyes Data Corporation, New Jersey: 1981

11. Gray, F.M. Solid Polymer Electrolytes: Fundamentals and Technological Applications, VCH Publishers, Inc, USA: 187-190; 1991.

12. Oosawa, F. Polyelectrolytes, Marcel Dekker, Inc, New York: 1971

13. Ott, L.S.; Hornstein, B.J.; Finke, R.G.; *Langmuir* **2006**, 22, 9357-9367.

14. Kuo, S.W.; Huang, C.F.; Wu, C.H.; Chang, F.C. *Polymer* **2004**, 45, 6613-6621.

15. Khougaz, K.; Clas, S.D. *J. Pharm. Sci.* **2000**, 89, 1325-1334.

16. Scheirs, J.; Bigger, S.W.; Then, E.T.H.; Billingham, N.C. *J. Poly. Sci.: Part B: Polymer Physics* **1993**, 31, 287-297.

17. Kim, J.H.; Min, B.R.; Won, J.; Kang, Y.S. *J. Phys. Chem.* **2003**, 107, 5901 – 5905.

18. Wu, H.; Wu, I.; Chang, F. *Polymer* **2001**, 42, 555-562.

19. PQS version 3.3, Parallel Quantum Solutions,2013 Green Acres Road, Fayetteville, Arkansas 72703

20. Becke, A.D. *J. Chem. Phys.* **1993**, 98, 5648.

21. Lee, C.; Yang, W.; Parr, R.G. *Physical Review. B* **1988**, 37, 785.

22. Cramer, C.J. In Essentials of Computational Chemistry*;* John Wiley & Sons Ltd: New York, NY, 2002, 268.

23. Dunning, T.H. Jr, *J. Chem. Phys.* **1989**, 90, 1007.

24. Gaussian 98, Revision A.7, Gaussian 98 (Revision A.7), M. J. Frisch, G. W. Trucks, H. B. Schlegel, G. E. Scuseria, M. A. Robb, J. R. Cheeseman, V. G. Zakrzewski, J. A. Montgomery, Jr., R. E. Stratmann, J. C. Burant, S. Dapprich, J. M. Millam, A. D. Daniels, K. N. Kudin, M. C. Strain, O. Farkas, J. Tomasi, V. Barone, M. Cossi, R. Cammi, B. Mennucci, C. Pomelli, C. Adamo, S. Clifford, J. Ochterski, G. A. Petersson, P. Y. Ayala, Q. Cui, K. Morokuma, D. K. Malick, A. D. Rabuck, K. Raghavachari, J. B. Foresman, J. Cioslowski, J. V. Ortiz, A. G. Baboul, B. B. Stefanov, G. Liu, A. Liashenko, P. Piskorz, I. Komaromi, R. Gomperts, R. L. Martin, D. J. Fox, T. Keith, M. A. Al-Laham, C. Y. Peng, A. Nanayakkara, C. Gonzalez, M. Challacombe, P. M. W. Gill, B. G.

Johnson, W. Chen, M. W. Wong, J. L. Andres, M. Head-Gordon, E. S. Replogle and J. A. Pople, Gaussian, Inc., Pittsburgh PA, 1998.

25. Vyazovkin, S.; Clawson, J.S.; Wight, C.A. *Chem. Mater*. **2001**, 13, 960-966

AMMONIUM NITRATE-POLYMER GLASSES: A NEW CONCEPT FOR PHASE AND THERMAL STABILIZATION OF AMMONIUM NITRATE

by

ANTHONY J. LANG AND SERGEY VYAZOVKIN

Journal of Physical Chemistry B 2008, 112, 11236–11243

Format adapted and errata corrected for dissertation

Abstract

Dissolving of ammonium nitrate in highly polar polymers such as polyvinylpyrrolidone and/or polyacrylamide can result in the formation of single phase glassy solid materials, in which NH_4^+ and NO_3^- are separated through an ion-dipole interaction with the polymer matrix. Below the glass transition temperature of the polymer matrix the resulting materials remain phase and thermally stable as demonstrated through the absence of decomposition as well as the solid-solid transition and melting of AN. The structure of the materials is explored by FTIR spectroscopy and density functional calculations. Differential scanning calorimetry, thermogravimetry, and isoconversional kinetic analysis are applied to characterize the thermal behavior of the materials.

Keywords: polyvinylpyrrolidone, polyacrylamide, thermal degradation, isoconversional kinetics, density functional, DSC.

Introduction

A widely used solid energetic material currently employed for propulsion is ammonium perchlorate (AP). However, AP decomposition yields high quantities of hydrochloric acid, which is highly detrimental from an environmental standpoint. In an effort to move towards cleaner burning solid propellants, many alternative routes have been explored, one example being ammonium nitrate (AN).[1,2,3,4,5] AN has sparked a great deal of renewed interest as its major decomposition products, water and nitrous

oxide,[3] are environmentally benign. It is also easily produced in mass quantities and rather stable to shock[4,5].

However, AN does present drawbacks, which include its solid-solid phase transitions within the storage temperature range as well as near its decomposition temperature, and, to a lesser extent, lower energy yields. AN has four solid-solid phase transitions in its operational temperature range which occur at -17, 32, 84, and 125 °C,[6,7,8,9] the most relevant of which is at 32 °C. At this temperature, AN undergoes a phase IV→III transition, which is a transition between two different orthorhombic crystal lattices. This transition involves a significant thermal effect as well as a drastic volume change, which presents a problem with the propellant industry, manufacturing, and storage of the material. The large volume changes lead to the material cracking, which causes irregular burn properties and also presents a possible threat to the propellant housing. In terms of storage, one must also consider the build-up of internal pressure and self-heating within the material, both of which can lead to disastrous consequences.

AN decomposition begins around 120°C[10] with a dissociative sublimation step via proton transfer from NH_4^+ to NO_3^- (eq. 1). The final products of the decomposition reaction are known[6] to be N_2O and H_2O.

$$NH_4NO_{3(s)} \rightarrow NH_{3(g)} + HNO_{3(g)} \rightarrow N_2O_{(g)} + 2H_2O_{(g)} \quad (1)$$

A possible mechanism for the proton transfer reaction has been explored theoretically by Alavi and Thompson,[11] who proposed that the transfer is promoted by the formation of gas phase clusters.

AN is used quite often as a propellant in the phase stabilized form (PSAN). PSAN is a mixture of AN and several wt. % of a metal oxide[12,13,14] such as zinc, nickel or copper

oxide, which is prepared via adding the metal oxide to melted AN (m.p. is ~170 °C[15]). PSAN exhibits very little volume change on thermal cycling. This effect is achieved by suppressing the formation of the phase III and, therefore, a solid-solid phase transition at 32°C.[14] Instead, the material undergoes an intermediate phase transition around 50°C, which has a heat release/absorption associated with it, but little volume change.

Although PSAN improves the utility of AN, the majority of AN is produced, stored, and used in unstabilized form as a fertilizer. In this form, AN remains prone to the aforementioned storage problems as well as makes it an explosive material readily available for terrorist attacks. A detailed list of incidents involving AN storage and usage has been compiled by Oxley et al[5]. In order to avoid the misuse of AN and its storage problems many types of mixtures have been prepared by adding various inert salts to AN. These mixtures are aimed at making AN nondetonatable, although they remain capable of a runaway reaction when stored in relatively small quantities (>1 kg)[5]

Although the use of PSAN may solve the phase transition problems, the problem of the low energy yields of AN remains. An increase in the energy yields is usually accomplished by the addition of common polymeric fuels/binders or high explosives.[16,17] Considering the fact that polymers are typically used in propellant formulations it would seem that the ultimate method of preventing the AN phase transitions would be to dissolve it into the polymeric binder material. A great deal of research has been performed on a class of polymers called solid polymer electrolytes that are employed for many applications ranging from batteries to drug delivery.[18,19,20,21] These materials make use of strong polar molecules incorporated into the backbone (i.e., polyethylene oxide) or into a side group (i.e. polyvinylpyrrolidone and polyacrylamide). These polymers are

capable of both hydrogen bonding and ion-dipole interactions with ionic salts such as lithium perchlorate, widely utilized in the battery industry, which may provide a platform to make efficient matrices for phase stabilization of AN. As an added benefit, many of these polymers have a low environmental impact and can be cast using water as opposed to flammable solvents.

In an earlier communication,[22] it was demonstrated that AN could be dissolved in the polyvinylpyrrolidone (PVP) matrix to generate a homogenous glassy material which prevents all of the solid-solid phase transitions in AN. Through such systems, it should be possible to prevent AN from undergoing detonation, as well as to control the temperature at which AN is released from the polymer matrix by controlling its glass transition temperature, T_g. This paper provides a detailed account of the thermal behavior of the AN-PVP system and also reports on characterization and behavior of a new system that makes use of a polyacrylamide (PAM) matrix for stabilization of AN. An objective of this work is to explore a novel concept of phase and thermal stabilization of AN by dissolving it in suitable polymer matrices.

Experimental

AN-PVP and AN-PAM samples were prepared in the form of thin films containing 0, 5, 10, 20, 25, 30, 40, and 50 wt. % of AN. PVP (molecular weights 8,000, 58,000, and 1,300,000 g mol^{-1}) and AN (99.9% purity) were purchased from ACRŌS Organics. PAM (molecular weight 5,000,000 g mol^{-1}) was purchased from Scientific Polymer Products, Inc. The AN-polymer films were prepared by combining the appropriate masses of AN and a polymer to bring the total mass to 0.5 g. The AN-PVP mixture was then dissolved in methanol, cast in 15 ml aluminum pans and allowed to dry

overnight under vacuum. AN-PAM mixtures were dissolved in deionized water, cast in 15 ml aluminum pans, and placed under vacuum till dry (typically 1.5-2 days). An Olympus polarized light microscope BX60 was utilized to examine the appearance of the films. Differential scanning calorimetry (DSC) was employed to monitor the solid-solid transitions, glass transition, as well as decomposition and degradation. These measurements were performed on a DSC 822^e manufactured by Mettler-Toledo. The temperature dependent mass loss during thermal degradation was monitored by a thermogravimetric analyzer (TGA). The TGA measurements were performed on a TGA/SDTA 851^e manufactured by Mettler-Toledo. For both TGA and DSC measurements, nonisothermal heating programs with an isothermal drying step were employed. The temperature was ramped from 25 to 115°C at 5 °C min^{-1}, and held at 115°C for 20 min in order to drive off any absorbed water or residual solvent. The heating program then continued to 550 °C at the following heating rates: 2, 5, 7, 9, 11, 13, and 15 °C min^{-1}. The data obtained from this second nonisothermal ramp of TGA measurements were subjected to isoconversional kinetic analysis, which, as discussed in a recent review paper,[23] provides a very effective approach to exploring complex kinetics in polymeric materials. The activation energy, E_α, as a function of the extent of conversion, α, was determined using the advanced isoconversional method developed by Vyazovkin.[24,25]

Fourier transform infrared spectroscopy (FTIR) measurements were performed on a Nexus 470 FTIR spectrometer manufactured by Thermo Nicolet. For AN-PVP and PVP, thin (~0.02 mm) films were cast onto KBr pellets and dried in an oven for 30 min at 100 °C. Since AN-PAM and PAM was cast using water as a solvent, they were deposited

onto Teflon cards ("ST-IR Cards" by Thermo Electron Corporation). A thin layer of PAM or AN-PAM solution was placed on the cards and allowed to dry in an oven for 30 min at 90 °C. The spectra were taken at 4 cm^{-1} resolution. For TGA-FTIR measurements the outlet of the TGA instrument was connected by a heated transfer line to a heated gas cell of the FTIR spectrometer. In an attempt to visualize the spatial arrangement of AN to the polar functional groups of PVP and PAM, quantum mechanical structural calculations were performed utilizing density functional theory at the B3LYP/6-31G* level. These calculations were performed with Gaussian '03[26].

Results

DSC

DSC was employed to study the thermal properties of the AN-host polymer systems. Figure 1a is a typical result seen in DSC measurements for AN-PAM material. Presented are two curves, one of a 25% AN-PAM film and the other of pure AN. Observing the DSC trace of pure PAM, we can see the glass transition, which occurs around 185°C. Neat AN demonstrates three solid-solid transitions followed by melting. Figure 1b presents two curves, one of an AN-PAM ground powdered mixture (prepared by mechanically mixing AN with PAM with a mortar and pestle), and the other of an AN-PAM homogenous film cast from water. In the DSC experiments involving the homogeneous film, no thermal events occur except a slight disruption in the base line as the materials approaches the temperature region of PAM degradation. When looking at the powdered mixture of AN-PAM, one can clearly see a solid-solid phase transition as well as the melting of AN. These results are consistent with the previously reported observations for AN-PVP material.[22]

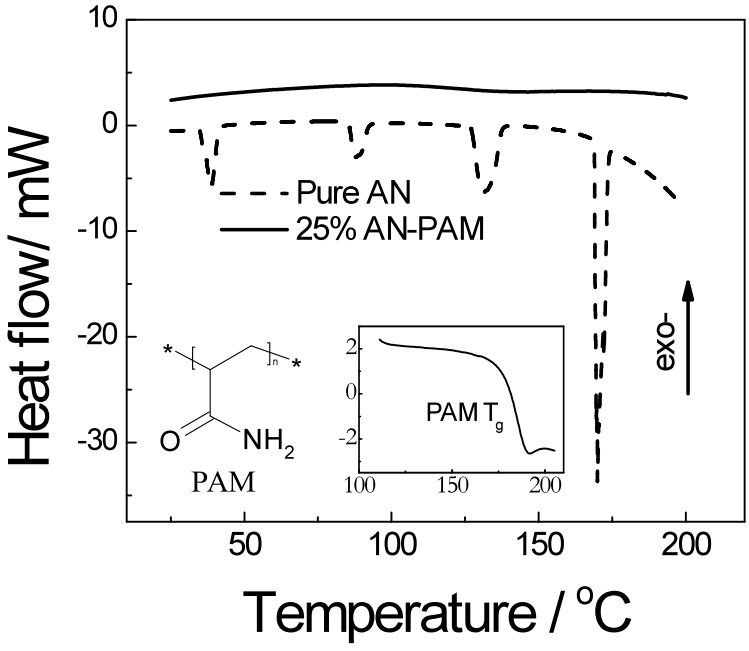

Figure 1a: DSC traces at 5 °C min^{-1} of PAM film containing 25 wt% of AN and neat AN (insets show PAM repeat unit and the glass transition in PAM).

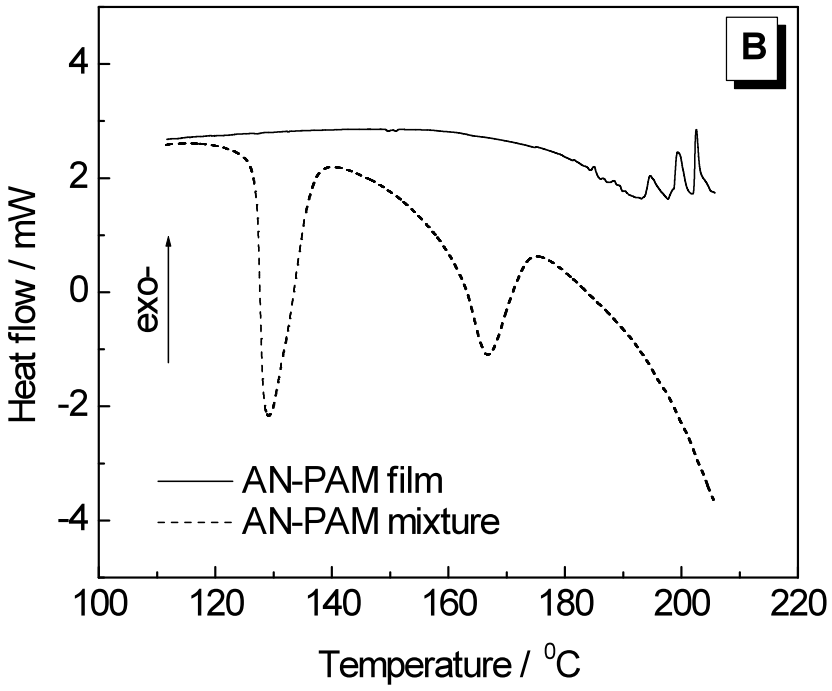

Figure 1b: DSC traces at 5 °C min^{-1} of PAM film containing 25 wt% of AN and a mechanically mixed powder 25 wt% of AN with PAM.

It should be mentioned that the phase transitions become detectable above a certain threshold loading. As seen in Figures 2a and 2b, this threshold value is above 25 wt. % of AN for both materials. Polarized light optical microscopy images (Figure 3za) indicate that at higher loadings the materials lose their homogeneity forming crystalline regions (Figure 3zb). Below the threshold both materials appear (Figure 3aZ) and behave as homogenous glasses, i.e., amorphous solids. Note that the threshold loading is consistent with the ratio of 1 molecule of AN per 2 molecules of PVP or PAM.

Figure 3 demonstrates the behavior of AN-PVP and AN-PAM (containing 25 wt. % AN) glasses when heated from 25 to 350 °C (at 5°C min^{-1}). In the AN-PVP system, a very strong exothermic peak is observed at ≈160°C, which is practically equal to T_g of the respective PVP matrix of the molecular weight 1,300,000 g mol^{-1}. A similar exothermic peak is also observed in the AN-PAM sample, however, the peak appears markedly above T_g.

FTIR

In order to further probe the interaction of AN with the polymer host, FTIR spectroscopy was employed (Figures 4a-c). Utilizing this technique, it is possible to detect an interaction of the ions with various functional groups in the polymer hosts. In Figure 4a, one can see a shift of the carbonyl stretch from 1650 cm^{-1} in neat PVP to 1680 cm^{-1} in AN-PVP sample. There is also a shoulder at the wavelength of the original carbonyl stretch. However, no shift is observed for carbonyl stretch in AN-PAM system (Figure 4b). Figure 4c identifies the symmetric (3207 cm^{-1}) and asymmetric (3342 cm^{-1}) stretches of $–NH_2$. It is seen that compared to neat PAM the symmetric stretch increases in the intensity in the AN-PAM system.

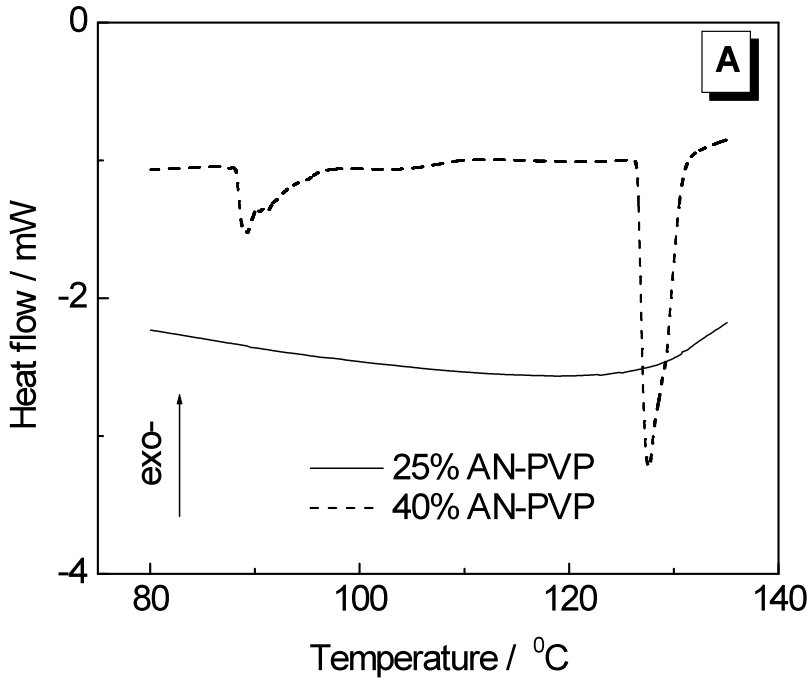

Figure 2a: DSC traces at 5 °C min^{-1} of AN-PVP films showing the effect of increasing AN load.

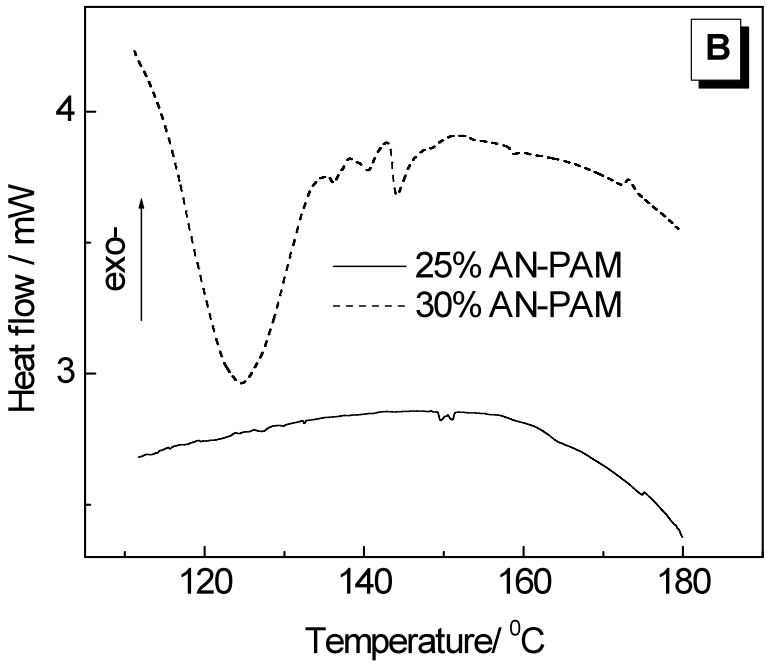

Figure 2b: DSC traces at 5 °C min^{-1} of AN-PAM films showing the effect of increasing AN load.

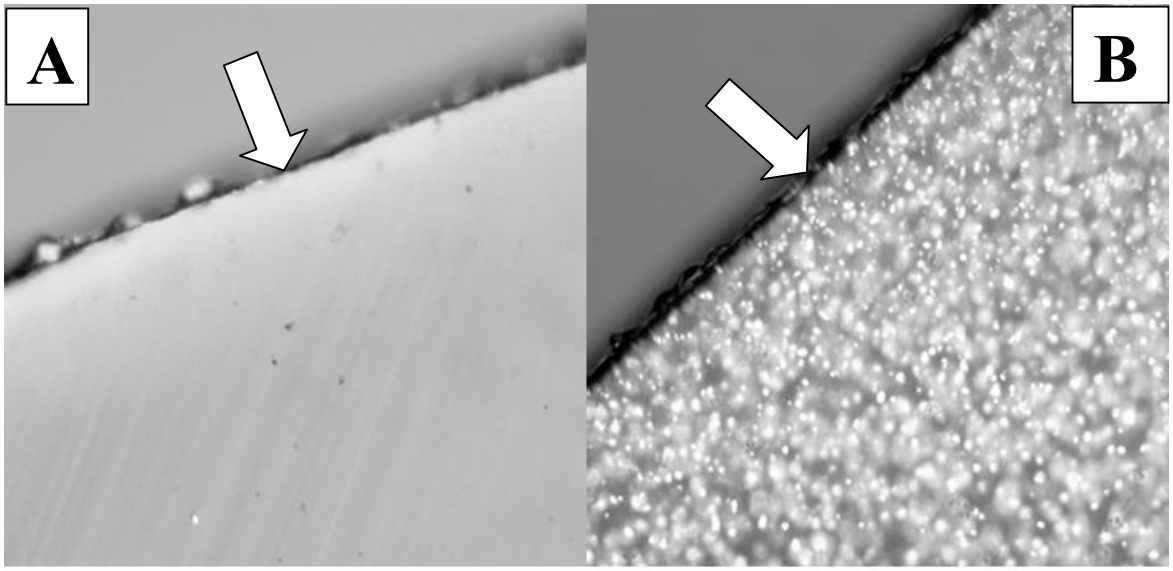

Figure 3Z. Polarized light microscopic images of AN-PVP films: (A) 25% AN-PVP and (B) 50% AN-PVP. Arrow shows the edge of the film. The actual size of individual images is 1mm x 1 mm.

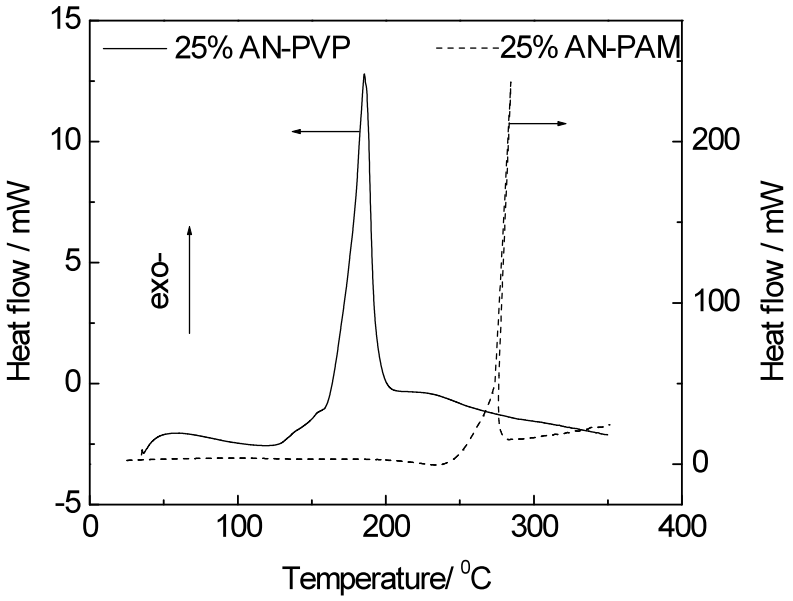

Figure 3: DSC traces of systems containing 25 wt% of AN in PAM and PVP heated from 25 to 350°C at 5 °C min^{-1}.

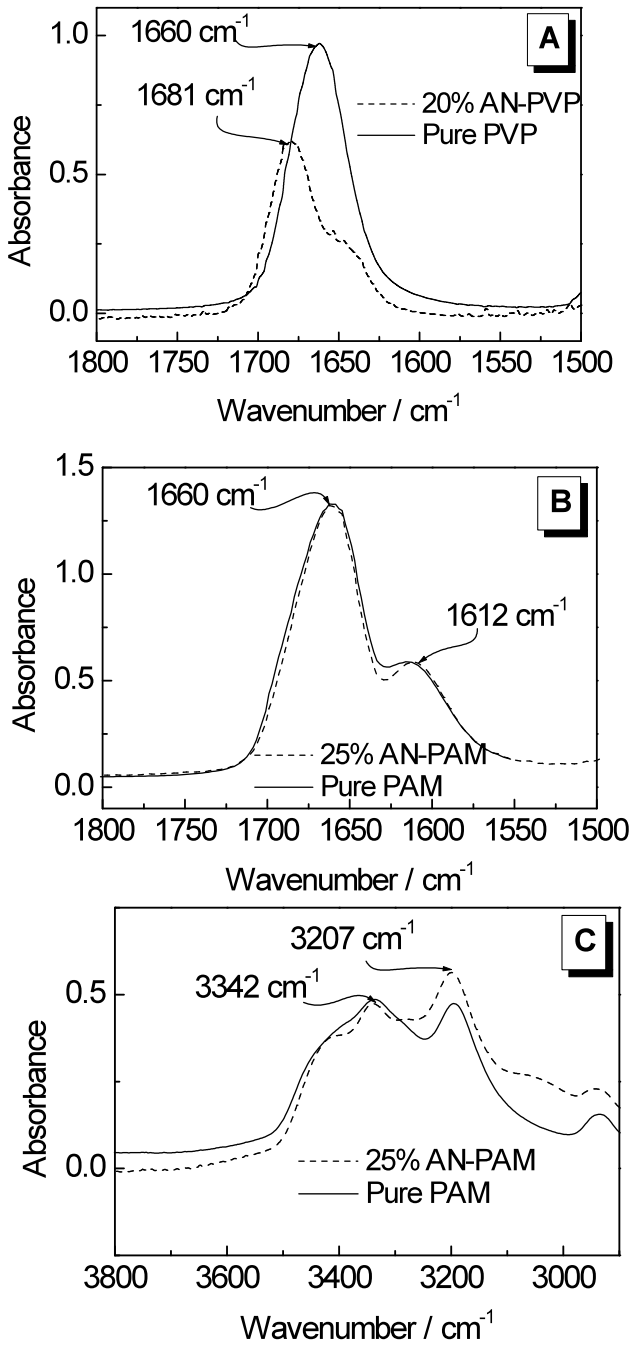

Figure 4: FTIR spectra for films of AN-polymer materials and neat polymers: a) carbonyl stretch in PVP and AN-PVP; b) the carbonyl stretch in PAM and AN-PAM; c) –-NH_2 stretches for pure PAM and AN-PAM.

TGA

TGA was used to visualize the effect of AN loading on the thermal behavior of AN-PAM and AN-PVP materials (Figures 5a and b). Figure 5b demonstrates the effect of varying the percent of AN in the AN-PVP samples. It is seen that at any percentage of AN, there is a mass loss equal to the mass of AN loaded into the film that occurs around 160°C (i.e., at T_g of PVP). FTIR analysis of the gases evolved during the mass loss has shown NH_3 (968 cm^{-1}) to be the major product. Reliable detection of HNO_3 was not possible because the strongest absorption band (asymmetric stretch at 1709 cm^{-1}) has markedly lower molar absorptivity[27] than the 968 cm^{-1} band in NH_3 and also overlaps strongly with the absorption bands of water released from the hygroscopic PVP matrix. The only detected product related to HNO_3 was NO_2 (absorption band at 1621 cm^{-1}). However, it was possible the mass loss is accompanied by an increase in the sample temperature, as detected by the DTA signal. In the case of PAM (Figure 5a), a somewhat different behavior is observed. Pure PAM starts to degrade at ~250°. In the AN-PAM samples, the onset of PAM degradation is immediately followed by a substantial mass loss practically equal to the percent of AN loaded into the film. This mass loss is also accompanied by a substantial increase in the sample temperature as in the case of the AN-PVP samples. After the exothermic mass loss step has completed in the AN-PAM system, degradation appears to proceed as in neat PAM.

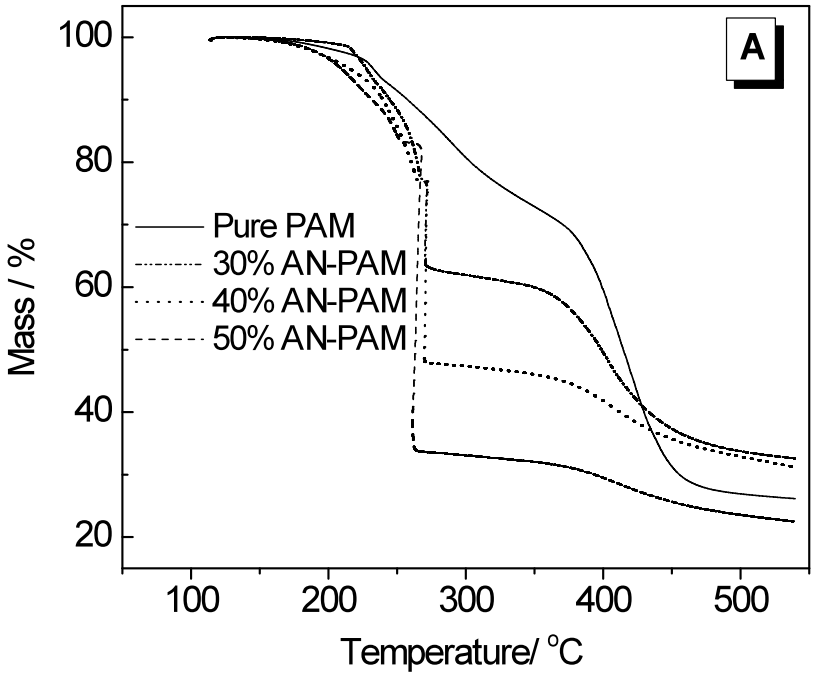

Figure 5a: TGA traces at 5 °C min^{-1} demonstrating the effect of increasing AN load in PAM-AN -systems.

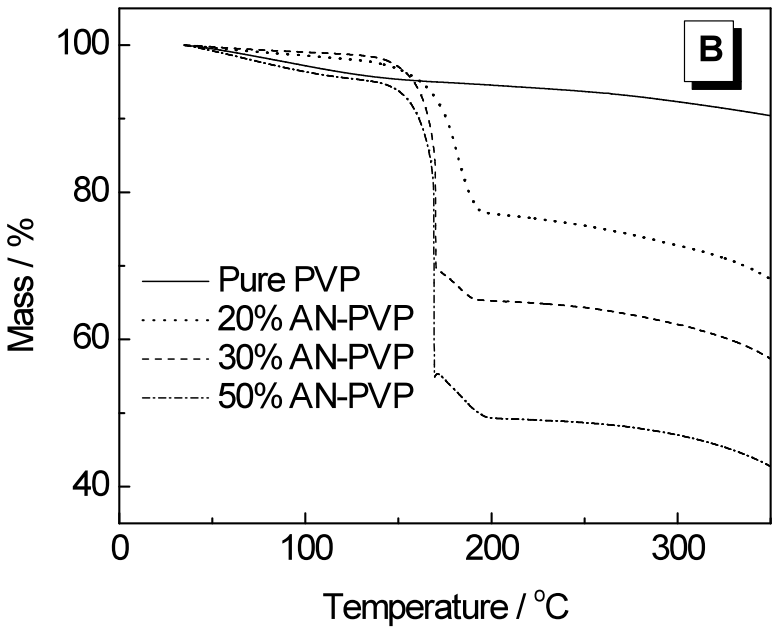

Figure 5b: TGA traces at 5 °C min^{-1} demonstrating the effect of increasing AN load in PVP-AN systems.

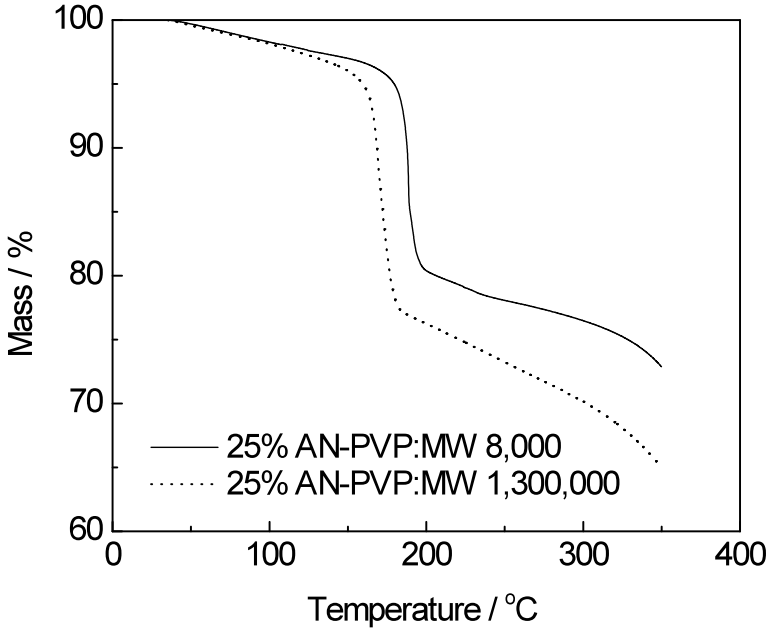

Figure 6: TGA traces at 5 °C min^{-1} tracking the mass loss of AN-PVP systems having PVP of different molecular weight (8,000 and 1,300,000 g mol^{-1}).

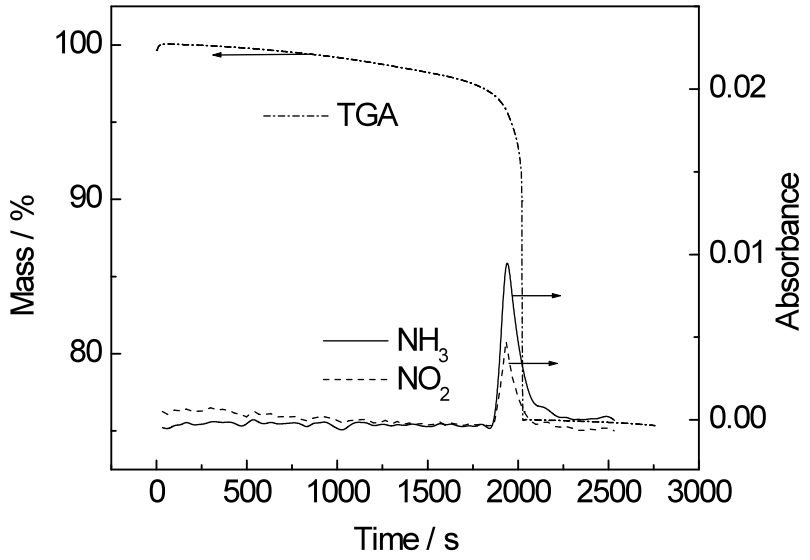

Figure 7: TGA-FTIR data demonstrating a release of gaseous NH_3 and NO_2 during the mass loss from an AN-PVP film.

A few runs have been conducted on AN-PVP materials made with PVP of different molecular weights in order to detect its effect on stability of the materials. Figure 6 illustrates the effect of changing the molecular weight of PVP in 25% AN-PVP systems. It is seen that changing the molecular weight of PVP from 8,000 to 1,300,000 g mol^{-1} has elevated the mass loss temperature of the AN-PVP materials by almost 20°C.

Kinetic calculations

The activation energy, with respect to the extent of conversion was determined from TGA mass loss data in order to probe the effect of AN decomposition on the thermal degradation of the residual polymer matrix. Figures 8 and 9 display a variation in the effective activation energy with the extent of conversion for the neat polymers and AN-polymer systems analyzed by the advanced isoconversional method.[24,25] For the thermal degradation of neat PVP (Figure 8) the initial E_α values are around 100 kJ mol^{-1} and increase until reaching a plateau of ~270 kJ mol^{-1} at $\alpha > 0.2$. In the AN-PVP system, it is difficult to determine the E_α values for the initial stages of mass loss, as degradation in the range of AN release is very unsteady. The later stages ($\alpha > 0.4$), however, demonstrate a plateau in effective activation energy at 190 kJ mol^{-1}. Figure 9 demonstrates the variation in activation energy with extent of conversion for PAM and an AN-PAM material. It is seen that both systems demonstrate the effective activation energies that gradually increase from ~70 to 270 kJ mol^{-1} with some discontinuity observed for AN-PAM systems during release of AN.

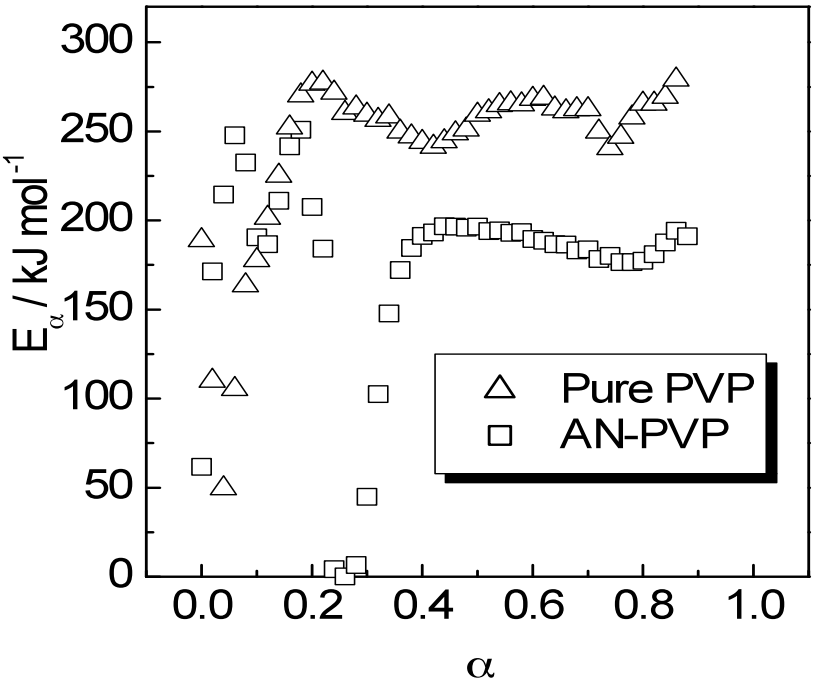

Figure 8: Dependencies of the effective activation energy on conversion for degradation of AN-PVP and PVP materials.

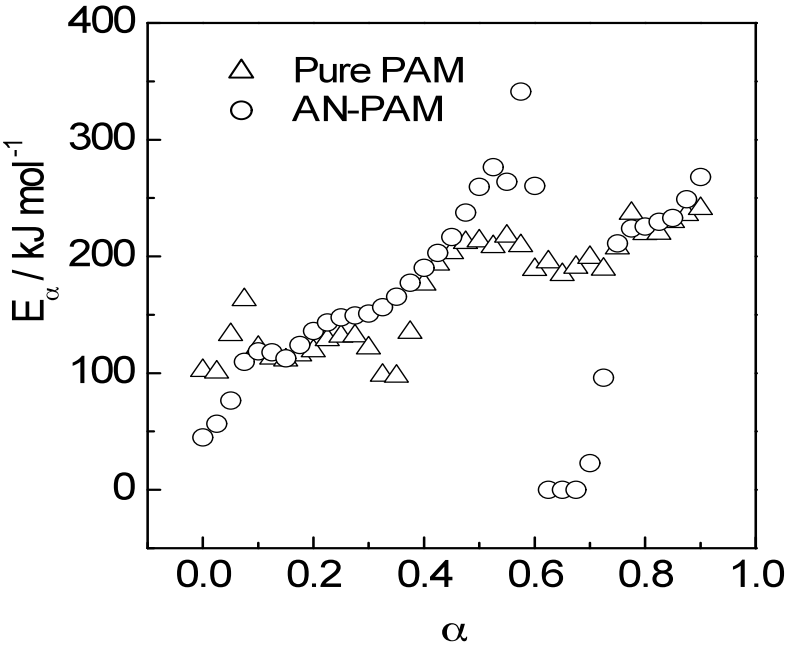

Figure 9: Dependencies of the effective activation energy on conversion for degradation of AN-PAM and PAM materials.

Theoretical structural calculations

Utilizing the density functional theory at a B3LPY/6-31G* level, PVP, PAM and AN-PVP, AN-PAM spatial arrangements were determined. The preliminary structures subjected to the calculations were based upon experimental data obtained from DSC measurements. Recall that the threshold loading of AN in PVP and PAM materials is accomplished at a ratio of 1 molecule of AN per 2 monomer units of PVP and/or PAM. The first attempts to determine the spatial arrangement of the monomers were performed on systems where the monomer units were attached to each other, i.e. they were two consecutive segments of one polymer chain. This proved to be inaccurate as the calculation was unable to resolve a sensible structure. The resulting structures involved a proton transfer from NH_4^+ to the carbonyl of the amide, which formed NH_3 and an alcohol. After various attempts to resolve this issue, including the incorporation of the polymer dielectric constant to account for the polymers ability to act as a solvent, it was decided to try a different approach. As it turned out a model assuming two non-connected monomer units (i.e., the units either belong to different polymer chains or to the same chain, but are separated by several units) provided a reasonable structural solution, which supported both the loading threshold and a direct interaction between the amide and the AN ions. The results of calculations are presented in Figures 10-12.

In order to further probe the interactions of AN to the polymer matrix, energy calculations for the AN-PAM were performed by looking at the solvation energies of each individual component and comparing them to the whole system in question. Table 1 lists the solvation energies for the systems as two monomers, monomers with single ions and monomers with both ions.

A

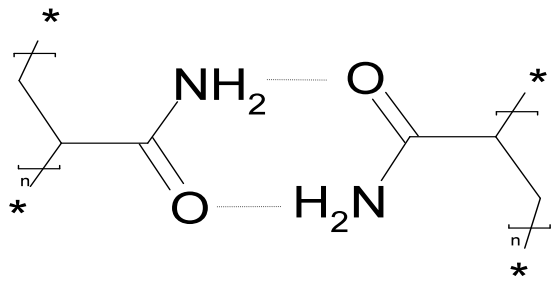

B

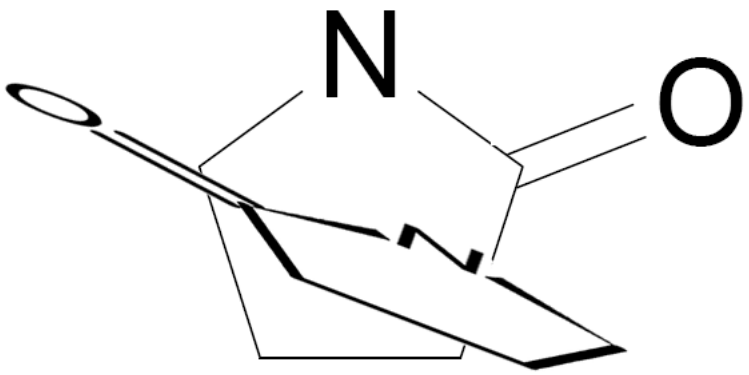

Figure 10: Computed structures of two monomers units for: a) PAM and b) PVP

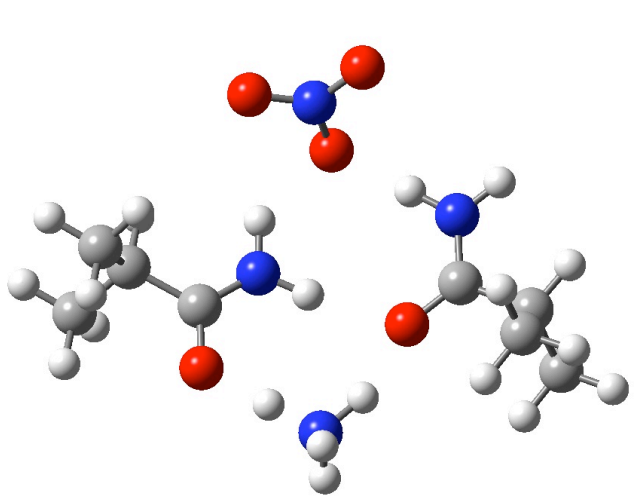

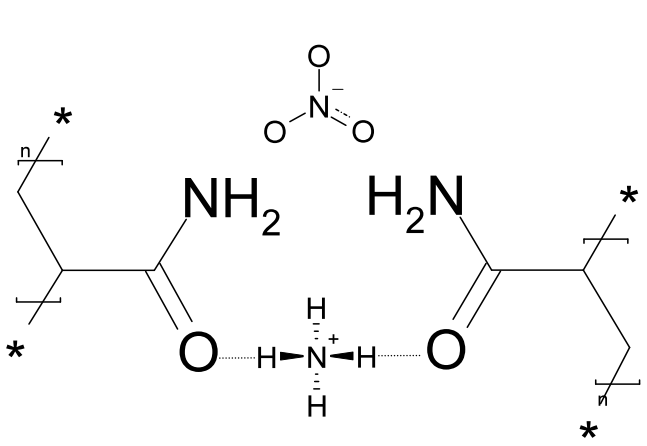

Figure 11: Computed structures for AN-PAM system: a) stereo and b) skeletal

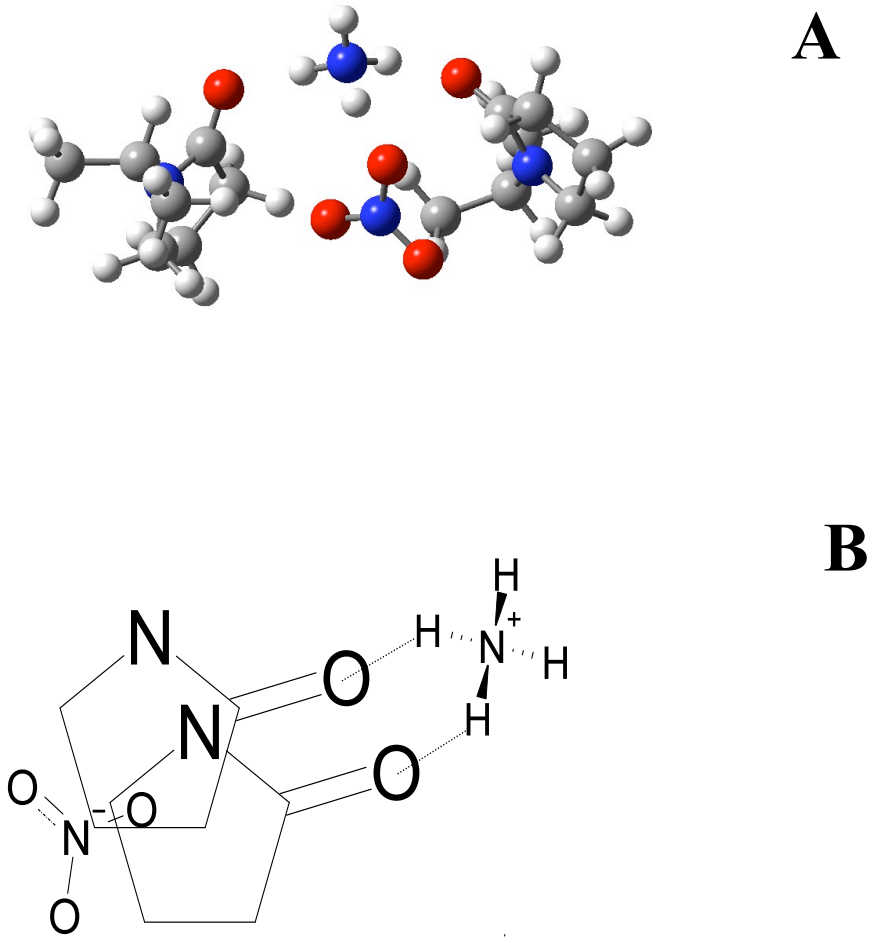

Figure 12: Computed structures for AN-PAM system: a) stereo and b) skeletal.

Table 1: AN-PAM theoretical results for the change in the interacting proton bond length of NH_4^+ ion, solvation energy for each of the systems and change in solvation energy for the complexes.

System	**N-H Distance/Å**	**E/kJ mol^{-1}**	**ΔE/kJ mol^{-1}**
2 Monomers		-1496995	
NH_4^+	1.027	-147955	
NO_3^-		-728989	
2 Monomers plus NH_4^+	1.084	-1645015	-65.4
2 Monomers plus NO_3^-		-2225942	-16.9
2 Monomers plus both ions	1.267	-2374365	-428.2

Discussion

An important aspect of this study is to demonstrate that various polymer matrices can be utilized in the formation of homogeneous glassy AN materials. It has been demonstrated that mixing PVP and AN can yield such materials.[22] In this study, PAM, a polymer that has an amide-containing side group as well as a notably high glass transition temperature, is examined to determine whether it provides a suitable matrix. From the DSC traces shown in Figure 1a it is clear that the T_g of pure PAM (bottom curve) is around ~180 °C. When PAM and AN are mixed mechanically via mortar and pestle solid-solid phase transitions associated with AN as well as its melting can be observed which indicates that PAM and AN are existing as two separate phases in the mixture (figure 1b). However, when AN is dissolved into PAM with water as a common solvent, it ceases to exist as an individual crystalline phase. Note that the mass of PAM and AN were the same in both the mechanical mixture and solvent cast samples. This suggests that PAM and AN are capable of forming amorphous glassy materials similar to the AN-PVP systems. An unexpected result is that when the AN-PAM glass is heated to higher temperatures we do not see either an exothermic peak or a mass loss related to AN until ~250 °C (Figure 3 and 6) which is ~60 °C higher than T_g of PAM. This is an obvious difference from the AN-PVP materials as they exhibit both thermal events at T_g of PVP (Figure 3 and 6).

AN-PVP materials have a dramatic mass loss step at T_g of PVP, where the mass loss is almost equal to the percent of AN in the matrix (figure 5a), and at this mass loss step we observe a dramatic heat release (figure 3). FTIR data of the gaseous products confirm that the mass loss is due to release of AN. The question that arises from this

result is whether the glass transition is the triggering event for the AN release. It certainly appears so, based on the TGA data for AN-PVP materials making use of PVP matrices of different molecular weights. It is well known[28] that increasing the molecular weight of a polymer generally results in increasing its glass transition temperature. TGA data shown in Figure 6 suggest that increasing the molecular weight of PVP from 8,000 to 1,300,000 g mol^{-1} results in increasing the temperature of the AN release by ~20°C which is consistent with increase in the T_g values of the respective PVP matrices. This indicates that the glass transition is the process triggering the release of AN from AN-PVP systems. This fact is consistent with a physical meaning of the glass transition temperature as the onset of long range cooperative motion of polymer chains. Below T_g the polymer chains experience only local mobility so that the AN ions, electrostatically bound to the PVP monomer units, remain separated from each other. Above T_g, the chain mobility intensifies increasing the probability of the ion interaction and proton transfer leading to the formation ammonia and nitric acid.

The above idea of the glass transition of a polymer matrix being a factor controlling the stability of an AN-polymer material also holds for AN-PAM systems. For the PAM matrix T_g is ~185°C, and AN-PAM materials do not show any phase transitions or degradation below this temperature (Figure 3 and 6). However, unlike the AN-PVP system, AN-PAM does not degrade immediately at T_g. As a matter of fact, AN-PAM starts degrading around 200 °C, i.e., at about the same temperature as neat PAM itself (Figure 6). The mass loss step associated with release of AN occurs at ~250°C, which is about 60°C above T_g of neat PAM. In order to explain this fact one should consider two phenomena. First, the T_g value of an AN-PAM system can be larger than that of neat

PAM. Second, an interaction of NH_4^+ and/or NO_3^- with PAM can be markedly stronger than with PVP so that it takes more thermal energy (larger temperature) to make proton transfer possible. At any rate, PAM appears to be a more effective matrix for stabilization of AN than PVP.

FTIR spectra (Figure 4) shed some light on the interaction of the AN ions with the polymers. A comparison of spectra (Figure 4a) for the carbonyl stretch from the amide in pure PVP and the AN-PVP systems suggests that in the latter the absorption band is shifted by 20 cm^{-1} toward higher frequencies. A shift to higher frequency is consistent with the idea of an ion-dipole interaction between the carbonyl group and NH_4^+. However, the AN-PVP spectrum also demonstrates a shoulder that lines up with the carbonyl absorption band in pure PVP (1650 cm^{-1}). Assuming that the shoulder represents unbound carbonyl stretching, one can conclude that some smaller fraction of the carbonyl groups does not take part in binding NH_4^+ ions. Nevertheless, a similar interaction is not observed in the AN-PAM system (Figure 4b) as the carbonyl band does not demonstrate any shift in this system compared to neat PAM. The only significant difference observed between PAM and AN-PAM spectra was an increase in the intensity of the symmetric–NH_2 stretch. However, it cannot be linked uniquely to the interaction between PAM and the AN ions because AN itself has a strong absorption band around 3200 cm^{-1}.[29] Perhaps, the interaction between the AN ions and PAM has a much more delocalized character than in the case of PVP where it is strongly localized on the carbonyl group.

It has been demonstrated that AN can form homogenous glassy materials with the two different polymers and that the resulting materials are thermally and phase stable up

to at least the glass transition temperature of the polymer matrix. Once AN is released from the polymer matrix, it does not obviously leave the remaining polymer intact. Overheated gaseous ammonia and nitric acid would cause both physical (bubbling, foaming) and chemical (oxidation, nitration) damage to the polymer matrix. If the polymers are to be used as propellant binders, a relevant practical question is how damage to the polymer matrix would affect its degradation kinetics and, in particular, the temperature sensitivity of degradation rate that is characterized by the effective activation energy. Figures 8-9 provide experimental values of the effective activation energy for the neat polymers as well as for AN-polymer materials. For PVP, the initial stages of degradation demonstrate lower activation energies as is commonly the case with degradation of polymers.[23] Initiation is followed by a propagation stage characterized by a plateau in the effective activation energy at ~270 kJ mol^{-1}. In the AN-PVP glass, the initial stages demonstrate irregular kinetics that does not lend itself for a reasonable interpretation. The later stages ($\alpha > 0.4$), however, demonstrate a plateau in the effective activation energy at 190 kJ mol^{-1}. A decrease of 80 kJ mol^{-1} in the plateau values of E_α for degradation of PVP from an AN-PVP material suggests that significant damage to the polymer has occurred during the release of AN and that this damage has decreased the energetic barrier to degradation. On the other hand, according to the E_α dependencies presented in Figure 9, neat PAM and PAM from AN-PAM material have practically identical values of the effective activation energies throughout the whole range of conversions. It means that whatever damage has taken place in PAM on release of AN, it has not made a noticeable impact on the energy barrier to degradation of PAM.

The theoretical calculations provide further insights into interaction of AN with the polymer matrices. Density functional techniques were employed because they are very effective in determining ground state geometries[30]. Multiple calculations were performed with two monomer units individually as well as with single and both ions. Despite different initial placements of the two monomer units, the structure always predicted the same geometry, which led to that being chosen for further calculation with only one ion and, then, with both ions.

For the neat PAM system, the favored orientation of the monomer units is to align in such a manner that the carbonyl of one monomer is in close proximity to the amine of the other as demonstrated in Figure 10. When the AN ions are added to the system, the carbonyls of the PAM monomers align themselves adjacent to each other in order to maximize contact with the NH_4^+ and NO_3^- ions (Figure 11a-b). It is noteworthy that in the AN-PVP system this does not occur. In the neat PVP system, the two monomers arrange themselves in a fashion such that there is no direct interaction between the amide group of each ring (Figure 10b). When attempting to uncover the lowest energy conformation for AN-PVP (Figure 12a) it was found that the NH_4^+ ion binds rather tightly to the carbonyls, and the NO_3^- ion is sandwiched in between the rings (demonstrated in Figure 12b). In this system the two AN ions are in close proximity to each other, more so than in the AN-PAM system. Given the close proximity of the ions to each other as well as the calculated orientation it is reasonable to expect that any increase in molecular mobility of the PVP matrix would readily result in the ions undergoing a proton transfer reaction that seems consistent with fact that AN is released from AN-PVP just above T_g of PVP.

Changes in the $H_3N—H^+$ bond length as well as changes in the solvation energy for the AN-PAM system are provided in Table 1. It is seen that the addition of any of the AN ions to the two monomers results in a noticeable decrease of the total system energy compared to the sum of the individual energies. The respective contributions are -65.4 kJ mol^{-1} for the NH_4^+ addition and -16.9 kJ mol^{-1} for the addition of NO_3^-. The decrease is significantly larger (-428.2 kJ mol^{-1}) when both ions are added. This result clearly stresses the energetic advantage of the formation of the AN-PAM complex involving NH_4^+, NO_3^- and two molecules of PAM. Another relevant effect is an increase in the $H_3N—H^+$ bond length. A minor increase (from 1.03 to 1.08 **Å)** occurs in the ammonia ion once it is put in contact with two monomer units of PAM. However, a truly significant increase (from 1.03 to 1.27 **Å**) is estimated to occur in the presence of NO_3^- and two molecules of PAM. This suggests that hydrogen bonding may play an important part in the interaction of NH_4^+ with the PAM and that this interaction should promote proton transfer.

Conclusions

The present study has covered multiple aspects of the formation, structure, and the thermal behavior of AN-polymer glassy materials. Although a better understanding of these materials would definitely require further investigations, the present work provides evidence of the new concept that polar polymer matrices can be used for phase and thermal stabilization of AN. AN incorporated in a polymer matrix is expected to be phase and thermal stable below the glass transition temperature of the matrix. For the polymers under study the AN load is limited by the ratio of one molecule of AN per two monomer units of the polymer. Nevertheless, larger loads might, in principle, be accomplished in

polymers, having multifunctional polar groups of a larger size. Polymer matrixes can also be tailored to specific applications of AN. For instance, fertilizer applications can be realized when using water-soluble and environmentally benign matrices such as PVP and/or PAM. On the other hand, energetic applications are envisioned through the use of nitrogen-rich matrix polymers that can serve as energetic binder/fuel.

Acknowledgement.

Thanks are due to Dr. Tracy Hamilton, Dmitry Zubarev, and Michael Marshall, for assistance with computations, to Amy Jablonski for data on degradation of neat PVP, to Dr. Kai Chen for assistance with FTIR measurements, and to Mettler-Toledo, Inc for the donation of the TGA instrument used in this work.

References

1. Simoes, P.N.; Pedroso, L.M.; Portugal, A.A.; Campos, J.L. *Thermochim. Acta*. **1998**, *319*, 55.

2. Rubtsov, Y.I.; Kazakov, A.I.; Lempert, D.B.; and Manelis, G.B. *Propell. Explos. Pyrot.* **2006**, *31*, 421.

3. Sayi, Y.S.; Yadav, C.S.; Shankaran, P.S.; Chhapru, G.C.; Ramakumar, K.L.; and Venugopal, V. *Int. J. Mass Spectrom.* **2002**, *214*, 375.

4. Sudhakar, A.O.; Mathew, S. *Thermochim. Acta*. **2006**, *451*, 5.

5. Oxley, J.C.; Smith, J.L.; Rogers, E.; Ming, Y. *Thermochim. Acta*. **2002**, *384*, 23.

6. Kubota, N. Propellants and Explosives, Wiley-VCH GmbH: Weinheim, 2002.

7. Turcotte, R.; Lightfoot, P.D.; Fouchard, R.; Jones, D.E.G. *J. Hazard. Mater.* **2003**; *101*, 1.

8. Singh G.; Felix, S.P. *Combust. Flame.* **2003**, *135*, 145.

9. Oommen C.; Jain, S.R. *J. Therm. Anal.* **1999,** *55*, 903.

10. Vyazovkin, S.; Clawson, J.S.; and Wight C.A. *Chem. Mater*. **2001**, *13*, 960.

11. Alavi, S.; Thompson, D.L. *J. Chem. Phys.* **2002,** *117*, 2599.

12. Simoes, P.N.; Pedroso, L.M.; Portugal, A.A.; Campos, J.L. *Thermochim. Acta*. **2000,** *364*, 71.

13. Mathew, S.; Krishnan, K.; and Ninan, K.N. *Propell. Explos. Pyrot.* **1998,** *23*, 150.

14. Engel, W.; Fietzek, H.; Herrmann, M.; Kempa, P.B. *Mater. Sci. Forum* **2001,** *378-381*, 331-335.

15. CRC Handbook of Thermophysical and Thermochemical Data; Lide, D. R.; Kehiaian, H. V. Ed.; CRC Press: Boca Raton, 1994.

16. Zeman, S.; Shu, Y.; Friedl, Z.; and Vagenknecht, J. *J. Hazard. Mater.* **2005,** 121, 11.

17. Babu, E.S.; and Kuar, S. *Propell. Explos. Pyrot.* **2004**, *29*, 50.

18. Gray, F.M. Solid Polymer Electrolytes: Fundamentals and Technological Applications; VCH Publishers, Inc: USA, 1991.

19. Meltzer, Y.L. Water-Soluble Polymers: Developments Since 1978; Noyes Data Corporation: New Jersey, 1981, 12, 508-527.

20. Oosawa, F. *Polyelectrolytes*; Marcel Dekker, Inc: New York, 1971.

21. Ott, L.S.; Hornstein, B.J.; Finke, R.G. *Langmuir.* **2006**, 22, 9357.

22. Lang, A. J.; Vyazovkin, S. *Mater. Lett.* **2008,** 62, 1757.

23. Vyazovkin, S.; Sbirrazzuoli, N. *Macromol. Rapid Comm.* **2006**, *27*, 1515.

24. Vyazovkin, S. *J, Comput. Chem*. **1997**, *18*, 393-402.

25. Vyazovkin, S. *J. Comput. Chem*. **2001**, *22*, 178-183.

26. Gaussian 03, Revision D.01, M. J. Frisch, G. W. Trucks, H. B. Schlegel, G. E. Scuseria, M. A. Robb, J. R. Cheeseman, J. A. Montgomery, Jr., T. Vreven, K. N. Kudin, J. C. Burant, J. M. Millam, S. S. Iyengar, J. Tomasi, V. Barone, B. Mennucci, M. Cossi, G. Scalmani, N. Rega, G. A. Petersson, H. Nakatsuji, M. Hada, M. Ehara, K. Toyota, R. Fukuda, J. Hasegawa, M. Ishida, T. Nakajima, Y. Honda, O. Kitao, H. Nakai, M. Klene, X. Li, J. E. Knox, H. P. Hratchian, J. B. Cross, V. Bakken, C. Adamo, J. Jaramillo, R. Gomperts, R. E. Stratmann, O. Yazyev, A. J. Austin, R. Cammi, C. Pomelli, J. W. Ochterski, P. Y. Ayala, K. Morokuma, G. A. Voth, P. Salvador, J. J. Dannenberg, V. G. Zakrzewski, S. Dapprich, A. D. Daniels, M. C. Strain, O. Farkas, D. K. Malick, A. D. Rabuck, K. Raghavachari, J. B. Foresman, J. V. Ortiz, Q. Cui, A. G. Baboul, S. Clifford, J. Cioslowski, B. B. Stefanov, G. Liu, A. Liashenko, P. Piskorz, I. Komaromi, R. L. Martin, D. J. Fox, T. Keith, M. A. Al-Laham, C. Y. Peng, A. Nanayakkara, M. Challacombe, P. M. W. Gill, B. Johnson, W. Chen, M. W. Wong, C. Gonzalez, and J. A. Pople, Gaussian, Inc., Wallingford CT, 2004.

27. Brill, T. B.; Arisawa, H.; Brush, P. J.; Gongwer, P. E.; Williams, G. K. *J. Phys. Chem*. **1995**, *99*, 1384-1392.

28. Sperling, L.H., Introduction to Physical Polymer Science; John Wiley & Sons Inc: Canada, 3rd ed. 2001.

29. http://webbook.nist.gov

30. Cramer, C.J. In*:* Essentials of Computational Chemistry; John Wiley & Sons Ltd: New York, NY, 2002, 268.

CONCLUSIONS

The present study has addressed the formulation, structure, and thermal behavior of ammonium-salt energetic materials. Through the use of isoconversional kinetics, it was determined that the effective activation energy for the various stages of decomposition are affected by sample preparation. It has been demonstrated that through the manipulation of the particle sizes, the density of pellets, and the pressure exerted, the thermal behavior of AP can be modified. The early stages of decomposition are associated with the formation of a sponge-like structure and variation on crystal size has little effect on this process, however when AP is formed into pellets via a hydraulic press, a different behavior is exhibited for the initial stages of decomposition. The later stage of decomposition under ambient pressure is predominately sublimation, while under high pressure or confined volumes (sealed pans) the sample undergoes a second gas phase exothermic decomposition. Under ambient pressures the later stage of decomposition can be characterized as having a steady state activation energy or a plateau. The value associated with this plateau changes significantly based on the sample preparation. When using large single crystals or pellets the plateau region's values are around 95 kJ mol^{-1}, however as the particle size decreases the activation energy of the plateau increases to 145 kJ mol^{-1}.

In order to further expand on the thermal behavior of ammonium-salt energetics, a novel material was developed, AN-polymer matrices. This material was developed in an attempt to improve the performance AN, using polymers systems. To better understand the properties of ammonium salt/polymers, the decomposition properties were analyzed. It was shown that through the use of polymers impregnated with ammonium nitrate, a

stable amorphous material can be produced, where the NH_4^+ and NO_3^- are completely separated. This is achieved due to the formation of ion-dipole bonds with the host. Two polymers were identified as adequate hosts, polyvinylpyrrolidone and polyacrylamide. Through these systems the formation of crystalline AN is prevented up to a maximum loading ratio, however above this ratio, crystal growth of AN is greatly limited which still provides for an excellent stabilizer. The benefit of such systems can be seen immediately through the elimination of AN's numerous phase transitions which are a major drawback of the material. An added benefit of this new type of formulation is the ability to control the temperature at which the respective cation and anion are able to recombine through the use of the polymer's molecular mobility restrictions. In the PVP-AN system it is shown that the recombination of the ions coincides with the T_g of PVP. However, in the PAM-AN system, recombination of the ions can only occur after substantial degradation to the polymer has occurred. This observation suggests that through clever polymer design one can control the temperature at which AN decomposes. It is also conceivable that if the host polymer is highly nitrated one can add to the decomposition properties, or by adding inert substituents its is possible to make AN-Polymer fertilizers, which are non-detonatable.

GENERAL REFERENCES

1. Galwey, A. K.; Brown, M. E.; Thermal Decomposition of Ionic Solids, Elsevier, Amsterdam, **1999.**

2. Boldyrev, V.V. *Thermochim. Acta* **2006** 443 1-36.

3. Vyazovkin S.; Wight, C. A. J. Phys. Chem. A **1997,** 101, (31) 5653-5658.

4. Vyazovkin, S.; Clawson, J. S.; Wight, C. A. *Chem. Mater*. **2001,** 13, 960-966.

5. Jacobs, P. W. M.; Ng, W. L. *J. Solid State. Chem.* **1974,** 9, 315.

6. Chang, F. M. ; Huang, C.C. ; Yeh, T.F. ; Liu, C.S. ; Leu, A.L. *Propellants, Explosives, Pyrotechnics* **1990,** 15, 261.

7. Manelis, G.B.; Nazin, G.M.; Rubtsov, Yu. I.; Strunin, V.A. Thermal Decomposition and Combustion of Explosives and Propellants, Taylor & Francis, London, 2003.

8. Bircomshaw, L.; Newman, B. *Proc. Roy. Soc.* **1955,** A227, 228–237.

9. Schultz, R.D.; Dekker, A.O. *J. Phys. Chem.* **1956,** 60, 1095.

10. P. Politzer; P.J. Lane, *Mol. Str. (Theochem)* **1998,** 454, 229.

11. Vyazovkin, S.; Wight, C. A. *J. Chem. Mater.* **1999,** 11, 3386-3393.

12. Waesche, R. H. W.; Wenograd, J. *Combust. Expl. Shock Waves*, **2000,** 36, 125.

13. Zhou, X.; Jackson, T. L.; Buckmaster, J. *Combust. Flame* **2003,** 133, 157.

14. Knott, G. M.; Brewster, M. Q. *Combust. Sci. Tech*. **2002,** 174, 81.

15. Panyam, R.; Price, R E.W.; Chakravarthy, S.R. *Combust. Flame* **2004,** 136, 1-15.

16. Simoes, P.N.; Pedroso, L.M.; Portugal, A.A.; Campos, J.L.; *Thermochim. Acta,* **1998,** 319, 1-2, 55-65.

17. Rubtsov, Y.I.; Kazakov, A.I.; Lempert, D.B.; and Manelis, G.B.; *Prop., Explos., Pyrotech* **2006**, 31, 6, 421-434.

18. Sayi, Y.S.; Yadav, C.S.; Shankaran, P.S.; Chhapru, G.C.; Ramakumar, K.L.; Venugopal, V. *Int. J. of Mass Spec* **2002**, 214, 3, 375-381.

19. Sudhakar, A.O.; and Mathew, S.; *Thermochim. Acta* **2006** 451, 1-2, 5-9.

20. Oxley, J.C.; Smith, J.L.; Rogers, E.; Ming, Y.; *Thermochim. Acta* **2002,**384,1-2, 23-45.

21. Kubota N, Propellants and Explosives, Wiley-VCH GmbH, Weinheim, 2002.

22. Turcotte R.; Lightfoot, P.D.; Fouchard, R.; Jones, D.E.G.; *J. Hazard. Mater.* **2003,** a101, 1-27.

23. Singh, G.; Felix, S.P.; *Combust. Flame* **2003**, 135, 145-150.

24. Oommen, C.; Jain, S.R.; *J. Therm. Anal.* **1999**, 55, 903-918.

25. Simoes, P.N.; Pedroso, L.M.; Portugal, A.A.; Campos, J.L. *Thermochim. Acta* **2000**, 364, 71-85.

26. Mathew, S.; Krishnan, K.; Ninan, K.N.; *Propellants Explos., Pyrotech*. **1998**, 23, 150-154.

27. Carvalheira, P.; Gadiot, G.M.H.J.L.; de Clerk, W.P.C.; *Thermochim. Acta* **1995** , 269/270, 273-293.

28. Zeman, S.; Shu, Y.; Friedl, Z.; Vagenknecht, J.; *J. Hazard. Mater.* **2005**, A121, 1-3, 11-21.

29. Babu, E.S.; Kuar, S.; *Prop., Explos., Pyrotech*. **2004**, 29, 1, 50-55.

30. Abthagir, P.S.; Saraswathi, R.; *Mater. Chem. Phys.* **2005**, 92, 21-26.

31. Meltzer, Y.L. Water-Soluble Polymers: Developments Since 1978, Noyes Data Corporation, New Jersey: pages 12 and 508-527; **1981.**

32. Gray, F.M. Solid Polymer Electrolytes: Fundamentals and Technological Applications, VCH Publishers, Inc, USA: Chapters 1,2 and pages 46, 187-190; **1991**.

33. Oosawa, F. Polyelectrolytes, Marcel Dekker, Inc, New York: **1971.**

34. Ott, L.S.; Hornstein, B.J.; Finke, R.G. *Langmuir* **2006**, 22, 9357-9367.

35. Kuo, S.W.; Huang, C.F.; Wu, C.H.; Chang, F.C.; *Polymer* **2004**, 45, 6613-6621.

36. Khougaz, K.; Clas, S.D.; *J. Pharm. Sci.* **2000**, 89, 1325-1334.

37. Scheirs, J.; Bigger, S.W.; Then, E.T.H.; Billingham, N.C.; *J. Poly. Sci. Part B: Polymer Physics* **1993,** 31, 287-297.

38. Kim, J.H.; Min, B.R.; Won, J.; Kang, Y.S.; *J. Phys. Chem*. **2003**, 107, 5901 – 5905.

39. Wu, H.; Wu, I.; Chang, F.; *Polymer* **2001**, 42, 555-562.

40. Vyazovkin, S.; *J. Comput. Chem*. **1997**, 18, 393.

41. Vyazovkin, S.; *J. Comput. Chem.* **2001,** 22, 178.

42. Brown, M.E.; Maciejewski, M.; Vyazovkin, S.; Nomen, R.; Sempere, J.; Burnham, A.; Opfermann, J.; Strey, R.; Anderson, H. L.; Kemmler, A.; Keuleers, R.; Janssens, J.; Desseyn, H. O.; Li, C.R.; Tang, T.B.; Roduit, B.; Malek, J.; Mitsuhashi, T. *Thermochim. Acta* **2000**, 355, 1-2, 125.

43. Brown, M.E. Introduction to thermal analysis , Kluwer Academic Publishers, Dordrecht, **2001.**

44. Peniche, C.; Zaldivar, D.; Pazos, M.; Paz, S.; Bulay, A.; San Roman, J. *J. Appl. Polym. Sci.* **1993**, 50, 485.

45. Lee, C.; Yang, W.; Parr. R.G.; *Physical Review. B* **1988**, 37, 785.

46. Cramer, C.J. In Essentials of Computational Chemistry; John Wiley & Sons Ltd: New York, NY, **2002**; 268.